



**US Army Corps
of Engineers®**
Engineer Research and
Development Center



ERDC 6.1 Basic Research

The Urban Ground-to-Ground Radio-Frequency Channel

Measurement and Modeling in the Ultrahigh Frequency Band

Daniel J. Breton, Caitlin E. Haedrich, Garrett R. Hoch,
Samuel S. Streeter, and Michele L. Maxson

July 2020



The U.S. Army Engineer Research and Development Center (ERDC) solves the nation's toughest engineering and environmental challenges. ERDC develops innovative solutions in civil and military engineering, geospatial sciences, water resources, and environmental sciences for the Army, the Department of Defense, civilian agencies, and our nation's public good. Find out more at www.erdclibrary.on.worldcat.org/discovery.

To search for other technical reports published by ERDC, visit the ERDC online library at www.erdclibrary.on.worldcat.org/discovery.

The Urban Ground-to-Ground Radio-Frequency Channel

Measurement and Modeling in the Ultrahigh Frequency Band

Daniel J. Breton, Caitlin E. Haedrich, Garrett R. Hoch, Samuel S. Streeter,
and Michele L. Maxson

*U.S. Army Engineer Research and Development Center (ERDC)
Cold Regions Research and Engineering Laboratory (CRREL)
72 Lyme Road
Hanover, NH 03755-1290*

Final Report

Approved for public release; distribution is unlimited.

Prepared for U.S. Army Corps of Engineers
Washington, DC 20314-1000

Under ERDC 6.1 Basic Research, PE 611102 / Projects T24 and 52C, "Wideband
Radio-Frequency Propagation in Urban Terrain"

Abstract

Ground-to-ground radio communication and sensing within the urban environment is challenging because line of sight between transmitter and receiver is rarely available. Therefore, radio links are often critically reliant on reflection and scattering from built structures. Little is known about the scattering strength of different buildings or whether such differences are important to the urban ground-to-ground channel. We tested the hypotheses that (1) diffuse scattering from built structures significantly impacts the urban channel and (2) scattering strength of urban structures varies with surface roughness and materials.

We tested these hypotheses by measuring urban channels in Concord, New Hampshire, and Boston, Massachusetts, and via channel-modeling efforts with three-dimensional representations of the urban environment. Direct comparison between measured and modeled channels suggest that both of these hypotheses are true. Further, it appears that ray-tracing approaches underestimate the complexity of urban channels because these approaches lack the physical processes to correctly assess the power incident on and scattered from built structures. We developed a radio-geospatial model that better accounts for incident power on both directly visible and occluded buildings and show that our model predictions compare more favorably with measured channels than those channels predicted via typical ray-tracing approaches.

DISCLAIMER: The contents of this report are not to be used for advertising, publication, or promotional purposes. Citation of trade names does not constitute an official endorsement or approval of the use of such commercial products. All product names and trademarks cited are the property of their respective owners. The findings of this report are not to be construed as an official Department of the Army position unless so designated by other authorized documents.

DESTROY THIS REPORT WHEN NO LONGER NEEDED. DO NOT RETURN IT TO THE ORIGINATOR.

Contents

| | |
|---|-------------|
| Abstract | ii |
| Figures and Tables | v |
| Preface | viii |
| Acronyms and Abbreviations | ix |
| 1 Introduction | 1 |
| 1.1 Background..... | 1 |
| 1.2 Objective..... | 3 |
| 1.3 Approach..... | 4 |
| 1.3.1 <i>Urban channel measurements</i> | 4 |
| 1.3.2 <i>Urban channel modeling</i> | 5 |
| 2 Assessment of the Urban Channel in Concord, New Hampshire | 6 |
| 2.1 Methods..... | 6 |
| 2.2 Results..... | 8 |
| 2.2.1 <i>Path loss</i> | 8 |
| 2.2.2 <i>Time dispersion</i> | 11 |
| 2.3 Conclusions..... | 14 |
| 2.3.1 <i>Path loss</i> | 14 |
| 2.3.2 <i>Time dispersion</i> | 14 |
| 2.3.3 <i>Small-city ground-to-ground channels</i> | 15 |
| 3 Measurement and Analysis of Ground-to-Ground Channels in Boston, Massachusetts | 16 |
| 3.1 Radio geospatial analysis..... | 16 |
| 3.1.1 <i>Horizontal components of bistatic range and delay</i> | 17 |
| 3.1.2 <i>Vertical components of bistatic range and delay</i> | 21 |
| 3.2 Channel sounding measurements..... | 23 |
| 3.2.1 <i>Methods</i> | 24 |
| 3.2.2 <i>Depolarization of the urban radio-frequency channel</i> | 25 |
| 3.2.3 <i>Radio-frequency channels in the urban core</i> | 27 |
| 3.2.4 <i>Radio-frequency channels adjacent to an urban core</i> | 30 |
| 3.3 Summary..... | 36 |
| 4 Radio-Frequency Channel Modeling | 38 |
| 4.1 Radio-frequency channel modeling with ray tracing..... | 39 |
| 4.1.1 <i>Short range, one turn (M8)</i> | 40 |
| 4.1.2 <i>Medium range, one turn (M21)</i> | 41 |
| 4.1.3 <i>Long range, two turn (M43)</i> | 42 |
| 4.1.4 <i>Summary of ray-tracing results</i> | 43 |
| 4.2 Urban covisibility studies with optical ray tracing..... | 43 |

| | | |
|----------|--|-----------|
| 4.3 | Building Raster Urban Channel Estimator (BRUCE): geospatial radio-frequency channel modeling via incident power profiles | 46 |
| 4.3.1 | <i>Vertical profiles of radio-frequency power incident on buildings</i> | 46 |
| 4.3.2 | <i>Total incident power for urban elevation profiles.....</i> | 50 |
| 4.3.3 | <i>Mapping building-incident and building-scattered power in urban terrain.....</i> | 53 |
| 4.3.4 | <i>Estimating the Urban Channel for the CRREL Channel Sounder.....</i> | 57 |
| 4.3.5 | <i>Comparison of measured and modeled power delay profiles.....</i> | 58 |
| 4.3.6 | <i>The constant cross-section assumption</i> | 62 |
| 5 | Conclusions..... | 65 |
| | References..... | 67 |
| | Report Documentation Page (SF 298)..... | 71 |

Figures and Tables

Figures

| | | |
|----|--|----|
| 1 | Sketch of a typical urban environment showing “direct,” specularly reflected, and diffusely scattered propagation paths..... | 2 |
| 2 | Handcart-mounted channel-sounder receiving unit in Downtown Boston, Massachusetts, with major components labeled | 4 |
| 3 | Map of rooftop-to-ground (<i>red</i>) and selected ground-to-ground (<i>blue</i>) channel measurement locations within Concord, New Hampshire | 8 |
| 4 | Log-log plot of path loss as a function of transmitter-to-receiver separation distance at 437 MHz in Concord, New Hampshire. The <i>straight lines</i> are least-square fits to the log-distance path loss model. Ground-to-ground antenna heights were 2.5 m, while the rooftop antenna was 15 m above ground level. Gray points are semitransparent to better show overlapping ground-to-ground and rooftop-to-ground data points..... | 10 |
| 5 | Example PDPs from Concord, New Hampshire, showing typical rooftop-to-ground (<i>left</i>) and ground-to-ground (<i>right</i>) channels. The <i>dashed red vertical line</i> is the minimum delay time | 12 |
| 6 | Root-mean-square delay spread vs. transmitter-to-receiver separation distance for ground-to-ground and rooftop-to-ground radio links in Concord, New Hampshire. Gray markers are semitransparent to better show overlapping ground-to-ground and rooftop-to-ground data points..... | 13 |
| 7 | Map of Back Bay with direct (<i>yellow line</i>) and scattered (<i>ellipses</i>) timings shown for the transmitter at TXBB and receiver at point O32. <i>Gray elliptical bands</i> , centered at 3.71 and 5.35 μ s delay times, are 80 ns (24 m) wide to show spatial resolution of the sounding system. The PDP in the <i>upper left</i> shows the expected free-space arrival time as a green vertical line and expected arrivals from the Prudential Tower and 200 Clarendon with <i>red</i> and <i>black lines</i> , respectively. Building color indicates, on a per-property basis, the relative building height from low (3 m; <i>dark purple</i>) to high (240 m; <i>white</i>)..... | 18 |
| 8 | Minimum-distant scatterer offset distance from the direct path versus the total transmitter-to-receiver separation distance for three different excess delay times..... | 19 |
| 9 | Delay-time corrections for 3-D paths in urban environments, as a function of horizontal separation distance and building height above ground level | 22 |
| 10 | Overview of Boston, Massachusetts, with relevant neighborhoods labeled and channel measurement sites indicated by <i>red points</i> | 24 |
| 11 | Comparison of collocated channel responses for three different polarizations. (a) Comparison of power delay profiles from a single location in Back Bay: vertically copolarized (VV), cross-polarized with the receiving antenna in cross-street orientation (VHx), and cross-polarized with the receiving antenna oriented parallel to the street (VHp). (b) Histograms of cross-polar discrimination (XPD) for the same location..... | 26 |
| 12 | Power delay profiles of co- (VV) and cross-polarized (VHp) signals for (a) point M262, which has LOS, and (b) point M294, which does not have LOS to the transmitter. (c) Map showing locations of the receiving points M262 and M294 relative to the transmitter, PS-TX. <i>Red lines</i> indicate the | |

| | | |
|----|--|----|
| | 1 μ s contours of constant bistatic delay time for M294, evaluated for 2-D distances..... | 28 |
| 13 | Map of the Back Bay neighborhood, showing the location of the transmitter site, study regions R1 through R4, and the three highest buildings along the High Spine. <i>Dots</i> indicate channel measurement points; <i>red-circled dots</i> are representative channels discussed in the text | 31 |
| 14 | Co- (VV) and cross-polarized (VHx) power delay profiles for point M012 in Back Bay study region R1. The <i>green vertical line</i> indicates the free-space arrival time, the <i>red vertical line</i> is the expected arrival from the Prudential Tower, and the <i>black vertical line</i> is the expected arrival from 200 Clarendon..... | 32 |
| 15 | Co- (VV) and cross-polarized (VHx) power delay profiles for point M032 in Back Bay study region R2. <i>Green, red, and black vertical lines</i> indicate expected free-space, Prudential Tower, and 200 Clarendon arrival times, respectively | 34 |
| 16 | Co- (VV) and cross-polarized (VHx) power delay profiles for point M043 in Back Bay study region R3. <i>Green, red, and black vertical lines</i> indicate expected free-space, the Prudential Tower, and 200 Clarendon arrival times, respectively. Weak returns from Downtown Boston can be observed starting at 12.8 μ s..... | 35 |
| 17 | Co- (VV) and cross-polarized (VHx) power delay profiles for point M057 in Back Bay study region R4. The <i>green vertical line</i> indicates expected free-space arrival time. The Prudential Tower and 200 Clarendon arrival times (<i>red and black vertical lines</i>) overlap at 5.6 μ s for this geometry. Strong returns from Downtown Boston start at 11.3 μ s..... | 36 |
| 18 | Virtual model used for ray-tracing studies of ground-to-ground channels in Back Bay, Boston. TX is the transmitter, and receiver points are indicated by labeled <i>yellow circles</i> . Not shown but present in the model is Downtown Boston, which lies across Boston Common in the direction indicated by the <i>blue arrow</i> | 40 |
| 19 | Modeled rays (<i>left</i>) and both modeled (<i>blue</i>) and measured (<i>orange</i>) power delay profiles (<i>right</i>) for receiver point M8..... | 41 |
| 20 | Modeled rays (<i>left</i>) and both modeled (<i>blue</i>) and measured (<i>orange</i>) power delay profiles (<i>right</i>) for receiver point M21..... | 42 |
| 21 | Modeled rays (<i>left</i>) and both modeled (<i>blue</i>) and measured (<i>orange</i>) power delay profiles (<i>right</i>) for receiver point M43, highlighted with the <i>red box</i> | 42 |
| 22 | Optical covisibility results from the RayCaster software for a small-scale urban environment. The ground-level transmitter (TX) is distant in the +Y direction, while the receiver (RX) lies at ground level between two buildings, as the <i>green arrow</i> indicates. The visibility state of various surfaces is indicated by color..... | 45 |
| 23 | Geometry for the vertical incident power profile analysis. Structures are shown in <i>black</i> and <i>gray</i> , structure dimensions are in <i>blue</i> , key parameters for diffraction analysis are in <i>green</i> , and the <i>red circle</i> indicates the test receiver position. For simplicity, this scenario does not include a secondary obstacle..... | 48 |
| 24 | The vertical profile for two different frequencies, expressed in decibels relative to free-space path loss (FSPL) of the power incident upon a hypothetical 200 m tall building. The controlling obstacle is 25 m tall, lies | |

| | | |
|----|--|----|
| | 200 m away from the transmitter, and is 800 m from the building..... | 49 |
| 25 | Elevation (<i>blue</i>) and gradient (<i>orange</i>) profile from the North End to Downtown Boston, Massachusetts | 51 |
| 26 | Elevation profile (<i>top</i>) and building face total incident power (<i>bottom</i>) for a path from the North End to the center of Downtown Boston. The transmitter is indicated by the <i>red dot</i> , and locations of building faces of interest are indicated by <i>orange dots</i> | 52 |
| 27 | Map of building-incident power. The <i>blue circle</i> indicates the location of a transmitter operating at $P_t = 10$ W. <i>Colored pixels</i> indicate the total building-incident power in decibels relative to one milliwatt at a given location. The red box indicates the area shown in Fig. 28; the large blank area in the lower left is the open space of Boston Common | 55 |
| 28 | Map of buildings and building-incident power. <i>Lighter shades of gray</i> indicate taller buildings, while <i>warmer-colored pixels</i> indicate higher power..... | 56 |
| 29 | Map of building-incident power with 1 μ s bistatic delay contours overlaid (<i>left</i>) and comparison of measured and modeled PDPs (<i>right</i>) for point M212. The <i>vertical green line</i> indicates the expected free-space signal delay time | 59 |
| 30 | Map of building-incident power and 1 μ s delay contours (<i>left</i>) and comparison of measured and modeled PDPs (<i>right</i>) for point M010. The <i>black vertical dashed lines</i> indicate expected arrival delays for signals scattered from the Prudential Tower and 200 Clarendon..... | 60 |
| 31 | Map of building-incident power and 1 μ s delay contours (<i>left</i>) and a comparison of measured and modeled PDPs (<i>right</i>) for point M032..... | 61 |
| 32 | Surfaces of the Prudential Tower and 200 Clarendon | 62 |

Tables

| | | |
|---|--|----|
| 1 | Details of the Boston channel sounding campaign | 23 |
| 2 | Comparison of channel statistics for typical short-range LOS and NLOS channels in Downtown Boston..... | 29 |
| 3 | Ray-tracing model parameters..... | 40 |

Preface

This study was conducted for the U.S. Army Corps of Engineers under ERDC 6.1 Basic Research, PE 611102 / Projects T24 and 52C, “Wideband Radio-Frequency Propagation in Urban Terrain.” The technical monitor was Dr. M. Andrew Niccolai, Engineer Research and Development Center, Cold Regions Research and Engineering Laboratory (ERDC-CRREL).

The work was performed by the Signature Physics Branch of the Research and Engineering Division, ERDC-CRREL. At the time of publication, Dr. M. Andrew Niccolai was Branch Chief; and Mr. J. D. Horne was Division Chief. The Deputy Director of ERDC-CRREL was Mr. David B. Ringelberg, and the Director was Dr. Joseph L. Corriveau.

COL Teresa A. Schlosser was Commander of ERDC, and Dr. David W. Pittman was the Director.

Acronyms and Abbreviations

| | |
|---------|--|
| 2-D | Two-Dimensional |
| 3-D | Three-Dimensional |
| AC | Alternating Current |
| BRUCE | Building Raster Urban Channel Estimator |
| COLLADA | COLLABorative Design Activity |
| CRREL | Cold Regions Research and Engineering Laboratory |
| DC | Direct Current |
| ERDC | U.S. Army Engineer Research and Development Center |
| FSPL | Free Space Path Loss |
| KED | Knife-Edge Diffraction |
| LOS | Line of Sight |
| NLOS | Non-Line of Sight |
| PDP | Power Delay Profile |
| RCS | Radar Scattering Cross Section |
| RF | Radio Frequency |
| RMS | Root-Mean-Square |
| UHF | Ultrahigh Frequency |
| VHF | Very High Frequency |
| XPDP | Cross-Polarization Discrimination Ratio |

1 Introduction

1.1 Background

The propagation of radio waves in mountainous or urban (often referred to as complex) environments is notoriously difficult to predict because (1) direct line of sight (LOS) between a given transmitter and receiver pair is rarely possible and (2) such environments often provide many alternative paths (multipath propagation) for signals, typically involving reflection, diffraction, and scattering. Collectively, those signal interactions with the environment are known as the radio-frequency (RF) channel, whose impulse response quantitatively describes the impact of the complex environment on the fidelity of the received signal.

Urban RF propagation modeling is an active research area for cellular telephone and data providers and academic research groups. These researchers generally focus on frequencies near 1 GHz* and above and model small-spatial-scale (microcell) propagation for existing and future cellular-communications-network planning. These systems leverage numerous rooftop or building-face-mounted antennae connected to robust, high-capacity, wired networks for data backhaul to combat the challenging urban propagation environment. These antennae are often “tuned” to perform optimally at a permanent installation location and use careful power control to minimize both cochannel interference and the time dispersion of the channel.

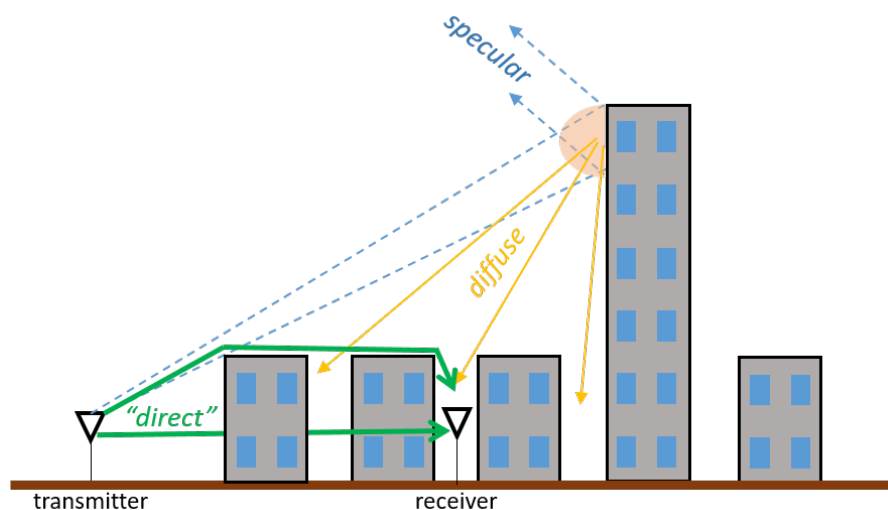
The urban RF-propagation problem faced by the Army (and potentially first responders responding to a disaster) is fundamentally different from cellular telephone service in spatial scale, RF frequencies, and accessibility to rooftops for safe or permanent antenna installations. Because of the typically lower antenna heights and omnidirectional antennae used by ground forces, the Army can expect to face heavier multipath conditions and more time-dispersed channels than cellular providers in urban environments. The fundamental urban channel of interest for the Army is perhaps the most challenging of all: the urban ground-to-ground channel.

* For a full list of the spelled-out forms of the units of measure used in this document, please refer to *U.S. Government Publishing Office Style Manual*, 31st ed. (Washington, DC: U.S. Government Publishing Office, 2016), 248–252, <https://www.govinfo.gov/content/pkg/GPO-STYLEMANUAL-2016/pdf/GPO-STYLEMANUAL-2016.pdf>.

Preparing for operations in urban areas is a major focus of the Army as communications cannot depend on existing wired or wireless commercial infrastructure to overcome the significant attenuation and dense multipathing observed on typical urban RF channels. Characterizing the geometry and material makeup of the propagation environment is critical, especially as previous studies (Driessen 1992; Devasirvatham 1988) have shown that signals scattered from both natural and built structures contribute significantly to the total RF power in non-line-of-sight (NLOS) conditions.

Several publications (Degli-Esposti and Bertoni 1999; Vitucci et al. 2012; Degli-Esposti et al. 2011) have discussed the importance of diffuse scattering in urban environments relative to the more commonly considered specular reflections, and this is especially true for the ground-to-ground channel. Assuming a ground-based transmitter, diffuse scattering from built structures allows for the redirection of the signal back down towards a ground-based receiver, whereas specular reflections are primarily directed up into the sky and cannot contribute to the ground-to-ground link, as shown in Figure 1. The so-called “direct” paths are rarely actual LOS paths but instead generally include both over-rooftop and urban-canyon propagation along an approximately straight line connecting transmitter and receiver. Such paths represent the closest approach to a truly direct LOS path allowed by the urban environment.

Figure 1. Sketch of a typical urban environment showing “direct,” specularly reflected, and diffusely scattered propagation paths.



RF propagation depends strongly on both the materials and geometry of the environment. In urban areas, both the materials and geometry are

generally man-made, hollow, and periodic. This allows potentially significant interaction with wavelength-scale features on their surfaces and deep penetration and reflections of RF waves inside these structures. These interactions are especially likely at the very high frequencies (VHF) and ultrahigh frequencies (UHF) relevant for military ground-to-ground and mobile-to-mobile communications.

Little is known about the relative diffuse scattering strength of different buildings as a function of surface roughness and cladding material or whether such differences are even important to the urban ground-to-ground channel. Existing propagation models typically assume flat, materially homogeneous buildings. Previous studies (Seidel et al. 1991; van Rees 1987) have discussed the range of radar scattering cross sections for buildings, but these works did not attempt to geospatially identify the scattering buildings or account for their surface and material structure.

1.2 Objective

Our work tested two hypotheses related to the urban ground-to-ground channel and commonly used urban channel estimation assumptions (flat, single-material buildings) discussed above.

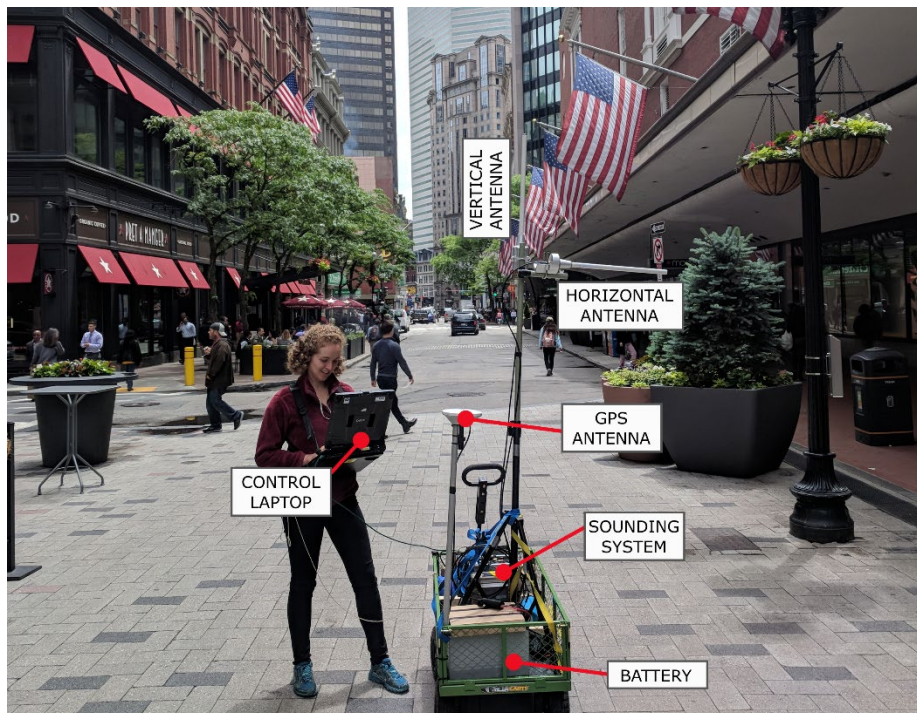
- Hypothesis 1: Diffuse scattering from built structures has significant impact on the ground-to-ground channel at frequencies relevant to military and first-responder operations. Here we define *significant impact* as the presence of radio reflections from built structures within 10 dB of the strength of the direct-path signal and with excess delay times greater than 1 μ s. Scatterers at excess delay times 1 μ s and greater generally lie outside of any canyon-mode propagation paths; we discuss this threshold in more detail in Section 3.1.1.
- Hypothesis 2: Diffuse scattering strength of urban structures depends on the surface roughness and materials present in the structures themselves. In essence, this hypothesis argues that not all buildings are equally important to the ground-to-ground urban channel.

1.3 Approach

1.3.1 Urban channel measurements

We conducted our initial field measurements in Concord, New Hampshire, in June 2017 and our main measurement campaign in Boston, Massachusetts, in June 2018. Our instrument was a portable channel sounding system developed at the Engineer Research and Development Center's Cold Regions Research and Engineering Laboratory (ERDC-CRREL) (Streeter, Breton, and Corgan 2018) operating at a center frequency of 440 MHz. This frequency is representative of tactical voice and data radio communications systems widely used by both military and first-responder organizations. The sounding system consists of separate transmitting and receiving units, each mounted in handcarts to enable easy navigation through streets and alleys as shown in Figure 2. The transmitting station sends a known pseudorandom code into the environment, and the receiving station records the incoming signal and measurement location. In postprocessing, the received signal is cross-correlated with the known signal, yielding a power delay profile (PDP), which characterizes and quantifies the urban channel existing between the transmitter and receiver points.

Figure 2. Handcart-mounted channel-sounder receiving unit in Downtown Boston, Massachusetts, with major components labeled.



1.3.2 Urban channel modeling

For our channel-modeling efforts, we first obtained from the Boston Planning and Development Agency both raster terrain elevation data and detailed three-dimensional (3-D) vector data describing the buildings of Boston. After locating our transmitter and receiver points within this geospatial dataset, we then applied three different approaches for urban channel modeling:

- An optical ray-tracing approach to identify and quantify areas of buildings simultaneously visible to both transmitter and receiver that might serve as scattering surfaces
- A commercially available RF ray-tracing model
- A geospatial raster-based approach that explicitly models both direct and diffracted contributions to RF power incident on buildings (This model, called the Building Raster Urban Channel Estimator [BRUCE], is discussed in detail in section 4.3.)

We draw our main conclusions for the project from comparing colocated channel measurements and modeled channels.

2 Assessment of the Urban Channel in Concord, New Hampshire

This section describes preliminary work performed in the relatively small, easily accessible city of Concord, New Hampshire. As this was our groups' first attempt at measuring the urban channel, our efforts in Concord aided us in equipment configuration and testing, provided an initial urban channel dataset to help develop radio-geospatial analyses appropriate for urban spatial scales, and enabled us to evaluate the impact of urban noise and interference on our channel measurements. Our subsequent ground-to-ground channel sounding campaign in Boston, Massachusetts, was successful based in large part on lessons learned, and insights into the urban channel gained, in Concord. We documented many aspects of the Concord work in Breton, Streeter, and Hoch (2018). Portions are reprinted here with permission from IEEE.

Previous studies (Cox 1973; Kalliola et al. 2003; Durgin, Kukshya, and Rappaport 2003) have taken many measurements of urban propagation in the 0.8 to 1.8 GHz range with the goal of understanding propagation between a mobile transceiver at ground level and an elevated base station. A few measurement campaigns (Devasirvatham 1988; Cheng et al. 2015) have focused on ground-to-ground radio links, and fewer still have examined frequency ranges relevant to military and first-responder operations where mobile-to-mobile communications must take the place of trunked or repeater-based infrastructure (Young et al. 2014).

Our goal in this work is to characterize the differences between the rooftop-to-ground and ground-to-ground urban channels using omnidirectional antennae at low UHF-band frequencies, focusing on trends in path loss and time dispersion. With respect to the main hypotheses, this section addresses the first hypothesis by attempting to answer the following question: Is the ground-to-ground channel significantly different from the elevated base station (or rooftop-to-ground) channel so widely studied in the literature?

2.1 Methods

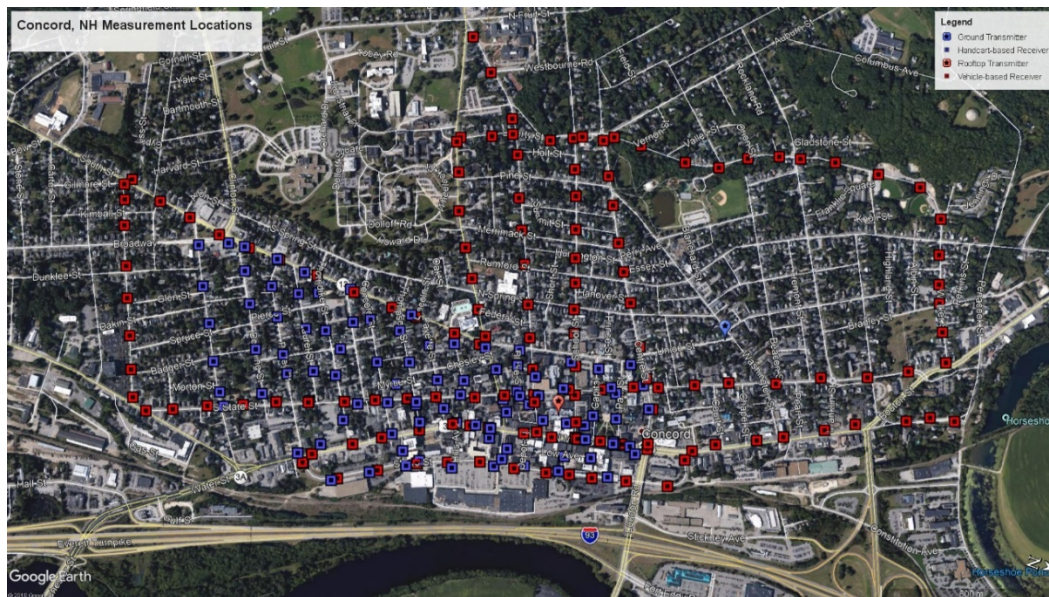
We used a portable channel sounding system operating at a center frequency of 437 MHz with a bandwidth of 25 MHz; Streeter et al. (2008)

provide system details. The transmitter and receiver terminals used identical omnidirectional broadband discone antennae and were synchronized in time and frequency using a GPS-disciplined rubidium oscillator. For the purposes of path loss determination, forward transmit power was measured on a Bird 7020 Power Sensor and recorded on a Bird 5000-XT data logger, while received power was measured with ± 1 dB accuracy at the sounding system receiver. Both the transmitter and the receiver were stationary for all measurements, and geographical positions were recorded using a standard GPS with ± 3 m accuracy.

Our urban site was Concord, New Hampshire, a relatively small urban area. At the city center, buildings are typically three to four stories tall, while outlying regions are predominantly one- to two-story, wood-framed, residential structures. We conducted ten rooftop-to-ground transects with the transmitter on top of an open-air parking garage, antenna height 15 m above ground level, while the receiver antenna was mounted at 2.5 m above ground level on top of a vehicle. The rooftop antenna was at a height comparable to most other rooftops within the urban core of Concord. Street widths, including on-street parking and sidewalks, are typically 20 m wide in Concord.

We conducted two ground-to-ground transects in June 2017 using vehicle-mounted and handcart-mounted systems. Antenna heights in both cases were 2.5 m above ground level. Subsequent handcart-based ground-to-ground transects (both transmitter and receiver antennae at 2.5 m above the ground) were performed in May 2018 to better sample the ground-to-ground channel and to ensure the rooftop-to-ground and ground-to-ground datasets were of comparable size. The measurement for both rooftop-to-ground and ground-to-ground points covered the core and outlying areas of Concord, as shown below in Figure 3.

Figure 3. Map of rooftop-to-ground (*red*) and selected ground-to-ground (*blue*) channel measurement locations within Concord, New Hampshire.



2.2 Results

2.2.1 Path loss

Path loss is the ratio of the power received to the power transmitted and therefore quantifies all signal losses (geometric spreading, diffraction, absorption, etc.) accrued between the transmitter and receiver points of a radio link. Because the received power can include both the desired signal and ambient noise, we must assess the contribution of noise to correctly determine path loss. We assessed noise levels through dedicated background measurements at selected locations and through analysis of shorter recordings of background levels prior to the arrival of the sounding signal. In Concord, we found very high noise levels along Pillsbury Street, which were related to the multiple studio-to-transmitter radio links located on the roof of the New Hampshire Public Radio headquarters building. Though the studio-to-transmitter links operate at a frequency well above the channel-sounder band and use highly directional antennae, harmonics and other inadvertent emissions are fairly common in the vicinity of transmitters. In our calculations of path loss in Concord, we discarded any measurement points with significant noise power, primarily those along Pillsbury Street.

Being a time-averaged quantity, the path loss combines the loss effects of the various multipaths composing a given channel. The literature contains

a number of models for urban propagation (Allsebrook and Parsons 1977; Hata 1980; Bertoni et al. 1994), and such models are often based on the concept of a path loss exponent, n . Using the log-distance model as an example (Rappaport 2002), path loss can be expressed as

$$L = L_0 \left(\frac{d}{d_0} \right)^n,$$

where

- L = the path loss at a source-receiver separation distance d ;
- L_0 = the reference path loss at a known distance d_0 ; and
- n = the path loss exponent, with values typically ranging from 2 to 4 in urban contexts.

Expressed in decibels, this above equation describes a straight line of slope n when plotted on log-log axes: $L_{dB} = L_{0,dB} + 10n \log_{10} \left(\frac{d}{d_0} \right)$.

Plotting our path loss values and least-squares lines fitted to the rooftop-to-ground data and to the ground-to-ground data, we obtain Figure 4. This figure shows remarkably similar path loss exponents of roughly $n = 2.8$ for both rooftop-to-ground and ground-to-ground datasets, though with a significant offset between them. The offset indicates that a ground-to-ground link typically suffers an additional 16 dB of path loss over an equivalent-length rooftop-to-ground link.

We believe the sudden increase in observed path losses for rooftop-to-ground links beyond 1 km result from additional topographic losses for measurements made in the northern, lower-elevation end of the city (right side of Figure 3). A simple theoretical model for height gain, based on a two-ray model for large separation distances (Bertoni 2000), is

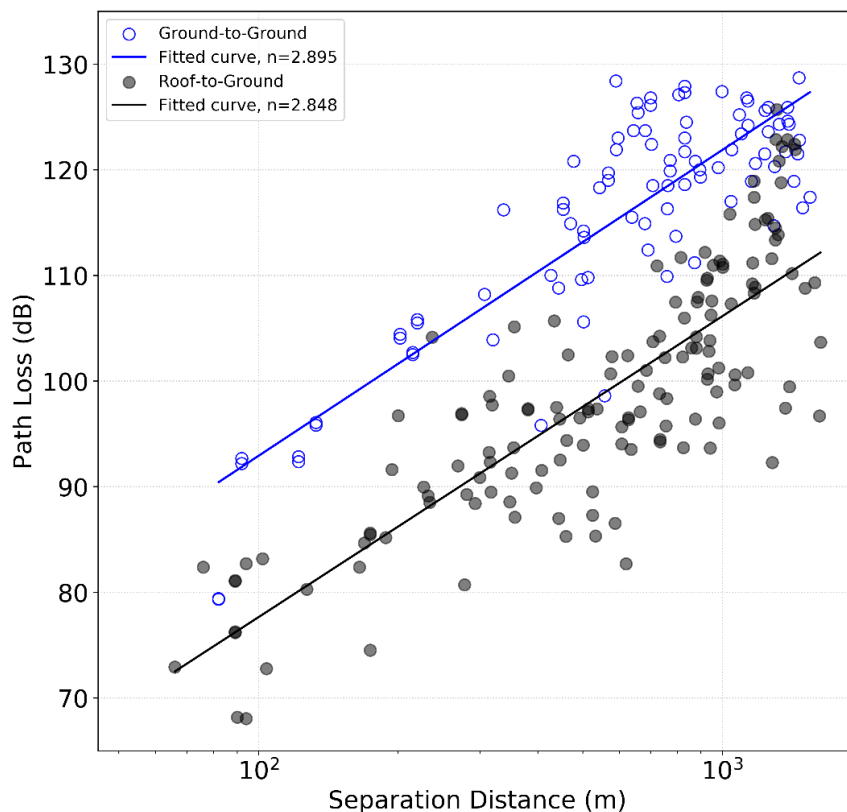
$$G_h = \frac{(h_1 h_2)^2}{d^4},$$

where

- G_h = the height gain;
- h_1 = the height above ground for antenna 1;
- h_2 = the height above ground for antenna 2; and

d = the antenna separation distance, expressed in the same units as h_1 and h_2 .

Figure 4. Log-log plot of path loss as a function of transmitter-to-receiver separation distance at 437 MHz in Concord, New Hampshire. The *straight lines* are least-square fits to the log-distance path loss model. Ground-to-ground antenna heights were 2.5 m, while the rooftop antenna was 15 m above ground level. Gray points are semitransparent to better show overlapping ground-to-ground and rooftop-to-ground data points.



Because of the simple multiplicative relationship, changing one antenna height in this model predicts a path loss curve parallel to the original curve, when losses are expressed in decibels. In the rooftop-to-ground scenario, the transmitter was $h_1 = 15$ m above ground level, and the receiver was $h_2 = 2.5$ m above ground level. In the ground-to-ground case, $h_1 = h_2 = 2.5$ m above ground level, leading to a predicted difference of about 15.6 dB between the two path loss curves at all distances.

The predicted value agrees well with our observed offset in Figure 4 of about 16 dB. However, our observed path loss exponent is 2.8 rather than the 4 assumed by the model; and given the many rough surfaces present in the urban environment, it is unlikely that the coherent reflections required

by the two-ray model are actually present. Other researchers (Allsebrook and Parsons 1977; Bertoni et al. 1994) have also pointed out that there is no expectation of the kind of coherent ground reflection required for the two-ray model to be valid in most urban scenarios. Despite the assumptions inherent in the theoretical height-gain model, it is clear from both a theoretical and experimental standpoint that (1) ground-to-ground links generally suffer greater path losses than rooftop-to-ground links and (2) the antenna height-gain component of the overall path loss depends weakly, if at all, on the separation distance.

2.2.2 Time dispersion

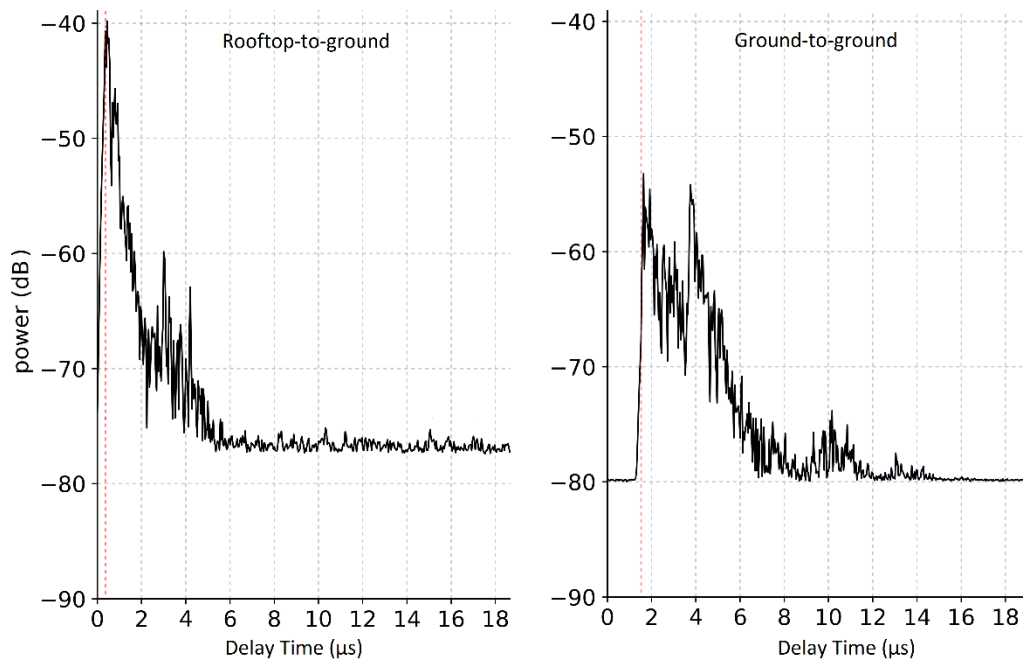
The principal output of a sounding system describing the time dispersion of the channel is the PDP. The PDP displays received power as a function of the time delay between transmission and reception of the various paths present in the channel. Because both units of our channel sounding system are equipped with GPS-disciplined rubidium oscillator clocks and because we synchronize our transmissions with the pulse-per-second output of the clock, we are able to record absolute delay times (Streeter, Breton, and Corgan 2018). Sounding systems lacking such synchronized clocks must rely on the presence of a clear LOS arrival to establish a timing reference, and such LOS paths are generally difficult or impossible to establish in complex terrain (Turin et al. 1972b).

The minimum possible delay time is simply the transmitter-to-receiver distance divided by the effective speed of light in air. Near-LOS paths will arrive within fractions of a microsecond of this minimum delay time. The maximum observed delay times depend on the limitations of the sounding system used and the nature of the propagation environment of interest. Significant paths with delays longer than 10 μs are rare in urban scenarios (e.g., Figure 5), while in mountainous terrain, delays longer than 60 μs can be common (de Weck 1988).

Figure 5 shows two typical PDPs to illustrate the main differences between the rooftop-to-ground and ground-to-ground channels. For the rooftop-to-ground channel shown, a direct-path arrival at the minimum delay time dominates the channel, with a “tail” of mostly indistinct reflected arrivals out to about 6 μs where the PDP merges with the noise floor. The example ground-to-ground channel shows a weak direct-path arrival emerging from the noise floor at 1.8 μs and a reflected path at 3.9 μs nearly equal in power to that of the direct path. Note that the noise floors for these two

measurements, taken approximately 250 m apart, are not the same: the rooftop-to-ground recording was collected in a region with higher ambient RF noise than the ground-to-ground recording. Recent research (Haedrich and Breton 2019; Breton et al. 2019) has shown that significant spatial variations in ambient noise are common in urban environments and, as shown here, can negatively impact the ability to measure the channel (Salous 2013).

Figure 5. Example PDPs from Concord, New Hampshire, showing typical rooftop-to-ground (*left*) and ground-to-ground (*right*) channels. The *dashed red vertical line* is the minimum delay time.



The root-mean-square (RMS) delay spread is a commonly used summarizing statistic to describe the time dispersion of a given channel (Bertoni 2000) and is defined as

$$\tau_{\text{rms}}^2 = \frac{\int_0^{\infty} (t-t_0)^2 P_r(t) dt}{\int_0^{\infty} P_r(t) dt},$$

where

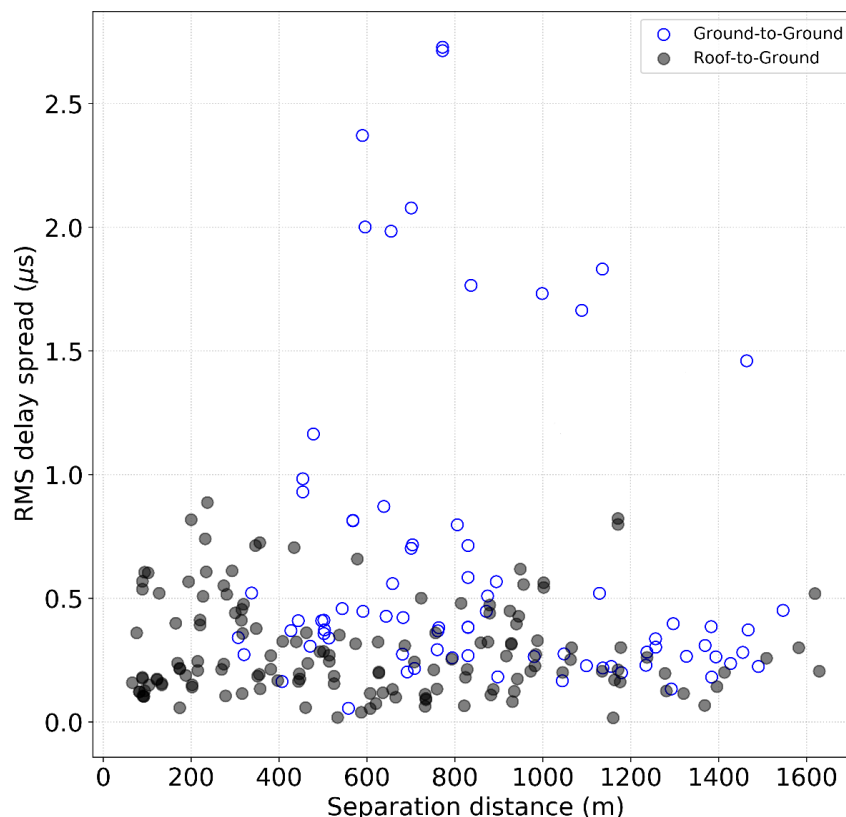
$$P_r(t) = \text{the received power at time } t \text{ and}$$

$$t_0 = \frac{\int_0^{\infty} t P_r(t) dt}{\int_0^{\infty} P_r(t) dt}, \text{ the mean excess delay.}$$

Because of the finite bandwidth (and thus nonzero sampling intervals) of practical channel sounding systems, the above integrals are typically replaced by summations in the analysis of actual data. The RMS delay spread can qualitatively be interpreted as a measure of channel complexity. Simple channels dominated by a single path will tend to have small values of RMS delay spread while complex channels with multiple returns of comparable power will have large values.

Figure 6 shows results for RMS delay spreads for both rooftop-to-ground and ground-to-ground links. The rooftop-to-ground links generally feature delay spreads smaller than $0.5 \mu\text{s}$, typical for elevated transmitters in urban scenarios, while the ground-to-ground links have a much greater variability and delay spreads regularly in excess of $1 \mu\text{s}$. Our delay spread results are generally consistent with those reported in Kozono and Taguchi (1993), though our data do not support their argument for an increasing RMS delay spread with separation distance.

Figure 6. Root-mean-square delay spread vs. transmitter-to-receiver separation distance for ground-to-ground and rooftop-to-ground radio links in Concord, New Hampshire. Gray markers are semitransparent to better show overlapping ground-to-ground and rooftop-to-ground data points.



2.3 Conclusions

2.3.1 Path loss

Path losses in urban environments are enormously variable due to the numerous opportunities for diffraction, multipath scattering, and absorption (Bertoni et al. 1994). Our work in Concord demonstrated that significant increases in path loss are incurred simply by moving one antenna from a rooftop to a ground elevation and that this change is likely independent from the separation distance. This result is consistent with theoretical predictions based on a two-ray model; though as discussed above, there is no reason why the urban environment should support the coherent reflections necessary for application of the two-ray theory.

It is unlikely that the additional path loss incurred by ground-to-ground links is borne equally by all of the multipaths composing the channel. In simple terrain with flat ground and an elevated transmitter, the paths carrying the most power are those closest to the direct LOS path. Assuming that the majority of signal power is carried along these nearly LOS paths, it also follows that such paths have the most power to lose and therefore have the greatest potential impact on the measured path loss. We believe that enhanced ground-to-ground path losses are indicative of losses predominantly affecting the earliest-arriving, highest-power, near-LOS paths.

2.3.2 Time dispersion

The hundreds of PDPs generated from our work in Concord are consistent with the spatial extent (roughly 3 km north to south) of the city itself. Received signal power generally merged with the noise floor inside of 10 μ s, with isolated reflections at longer delays, likely associated with the airport and other commercial structures standing on the other side of the Merrimack River.

Figure 5 demonstrates how the channel can change when the environment significantly limits the near-direct paths. Instead of a dominant direct-path arrival, now other paths, especially those involving distant scatterers, become comparable (or greater) in power to the near-LOS paths; and therefore, NLOS propagation becomes critical to understanding and effectively exploiting the channel. Other researchers have recognized this in a general sense (Kozono and Taguchi 1993; Seidel et al. 1991; van Rees 1987)

but generally have not sought to determine what and where these distant scatterers are.

2.3.3 Small-city ground-to-ground channels

Our work in Concord established that significant differences do exist between rooftop-to-ground and ground-to-ground channels, both in terms of path losses and time dispersion. Our channel measurements also showed that the structure of ground-to-ground channels in a small city can be influenced by the contributions of distant scatterers, leading to higher RMS delay spread values. In larger urban areas, distant scatterers influencing the channel are typically assumed to be tall buildings in locations directly visible by the transmitter or receiver (Seidel et al. 1991; van Rees 1987; Laurila et al. 2002). Despite the lack of high buildings in our study area and the highly restricted lines of sight available to either transmitter or receiver, our observations suggest that even distant, occluded structures can have an important influence on the ground-to-ground urban channel.

3 Measurement and Analysis of Ground-to-Ground Channels in Boston, Massachusetts

Boston, Massachusetts, founded in 1630, is one of the oldest cities in the United States and therefore features several geographically and architecturally distinct neighborhoods surrounding a comparatively small (approximately 1 km²) urban core known as Downtown. Buildings in the urban core are densely packed along irregular, curving streets and generally reach heights of 180 to 200 m. The two tallest buildings in New England stand apart from the urban core along the so-called “High Spine” of Boston overlooking the Back Bay neighborhood. The High Spine includes the 228 m tall Prudential Tower and the 240 m tall 200 Clarendon building, which feature prominently in the discussion of both channel measurements and modeling in Back Bay.

Our channel sounding campaign sought to characterize the urban ground-to-ground channel by using antenna heights, frequencies, transmit powers, and locations relevant to Soldiers and first responders (Vassiliou et al. 2013). The goal of the measurement campaign was to test our hypotheses on a wide variety of urban ground-to-ground channels. Boston, Massachusetts provided the geospatial variety necessary to test our ideas on many different urban channels, and conclusions drawn from these data and analyses are likely to be generally applicable for all urban areas.

We presented some of the following results at the 2019 National Radio Science Meeting (Breton, Haedrich, and Hoch 2019).

3.1 Radio geospatial analysis

To properly interpret channel sounding results with respect to their geospatial context, we have developed several geospatial tools to accurately describe and perform relevant propagation calculations for the unique urban geometries associated with each channel measurement point. In particular, the 3-D distances between transmitter, scatterers, and receiver are all critical to properly estimating the impact of a given scatterer on the measured channel. Significant errors can be introduced if the vertical components of signal paths are not considered, and this is especially true in complex, high-relief terrain such as cities.

Earlier work (Streeter, Breton, and Corgan 2018) in mountainous terrain simply calculated 3-D distances directly from the digital elevation model describing the terrain. For urban work, this approach is problematic due to the numerous sudden discontinuities in bistatic range associated with the urban landscape. For the current project, we therefore opted to divide our geospatial analyses into horizontal and vertical components as described below.

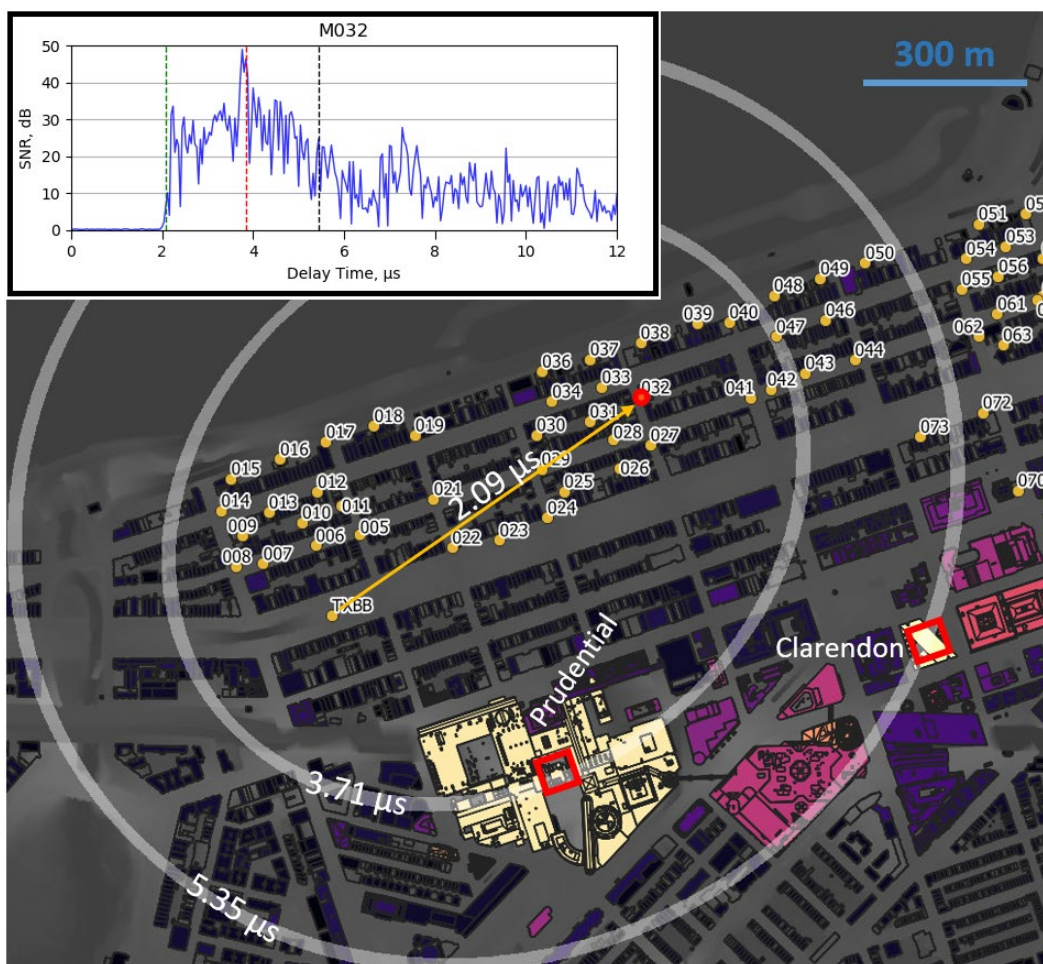
3.1.1 Horizontal components of bistatic range and delay

Urban geospatial data is typically composed of two parts: a raster “bare earth” ground digital elevation model and a vector representation of the structures standing atop that ground. In the course of channel sounding, our transmitter and receiver measurement points were determined via GPS, and can thus be properly geolocated (generally within ± 3 m in open environments, but occasionally as poor as ± 15 m in urban canyons; see Paulson 2019) within the raster and vector representations of the urban environment.

The RF channel is fundamentally a *bistatic phenomenon*, meaning that a signal produced by an emitter will travel out and interact with the environment in some way, and the results of that interaction will be received at a different location than that of the emitter. If we simplify the environment to having just one location for that interaction, then that location relative to the emitter and receiver positions determines the bistatic delay time required for the signal to travel from the emitter, to the interaction point, and over to the receiver. A given delay time does not define a unique location, however, but rather describes a 3-D ellipsoid (with emitter and receiver as foci) where the interaction could have occurred (Braun and Dersch 1991). Figure 7 shows examples of these constant delay-time contours overlaid on the urban scene.

Our sounding system is hardware limited to a 25 MHz bandwidth and, therefore, theoretically has a 40 ns timing and thus a 12 m spatial resolution. In practice, we assume an uncertainty of ± 1 timing bins and thus a spatial resolution of 24 m, a distance comparable to a street width. In other words, the scatterers separated by less than 80 ns of bistatic delay time could be combined in the same delay-time bin; such buildings cannot be spatially resolved by our sounding system (Salous 2013).

Figure 7. Map of Back Bay with direct (*yellow line*) and scattered (*ellipses*) timings shown for the transmitter at TXBB and receiver at point 032. *Gray elliptical bands*, centered at 3.71 and 5.35 μs delay times, are 80 ns (24 m) wide to show spatial resolution of the sounding system. The PDP in the *upper left* shows the expected free-space arrival time as a *green vertical line* and expected arrivals from the Prudential Tower and 200 Clarendon with *red and black lines*, respectively. Building color indicates, on a per-property basis, the relative building height from low (3 m; *dark purple*) to high (240 m; *white*).



Our sounding system uses omnidirectional antennae to more accurately capture the type of RF channel relevant to military and first-responder users. Because our antennae lack directivity, we can achieve spatial discrimination of scatterers in the environment only if we have (1) the absolute delay time of signal arrival, (2) accurate geospatial data describing the environment, and (3) accurate positioning data of our transmitter and receiver points.

Even if we meet all these requirements, it is still geometrically possible in an urban environment for multiple scatterers to fall within a given delay-time bin, making it impossible for us to distinguish the contribution of a

given scattering structure from the others. Nevertheless, this kind of analysis can often be useful in identifying the location of an obvious, isolated scatterer, as shown in the example on page 20.

A key aspect of our study is the ability to differentiate between the two main NLOS urban propagation modes: urban canyon propagation and contributions from distant scatterers (Laurila et al. 2002). In this report, *we define distant scatterers as those that arrive at or beyond 1 μ s excess delay time*. This definition is based on urban block geometry and the fact that the most likely contributors to canyon-mode propagation are one-turn (and less importantly, two-turn) paths through the urban environment (Bertoni 2000). For a classic rectilinear-type street grid, typical one-turn paths will stray no more than two block widths away from the direct path connecting transmitter and receiver. For smaller block widths (around 75 m, such as those observed in the Back Bay neighborhood of Boston), this minimum scatterer offset is therefore 150 m, and the shortest possible round trip covers 300 m. Because the speed of light in air is very nearly 300 m/ μ s, the round trip to the scatterer and back requires 1 μ s longer than the direct path (i.e., the scatterer has an excess delay of 1 μ s). For a given excess delay time, the scatterer offset distance depends on the overall transmitter-to-receiver separation distance, as shown in Figure 8.

Figure 8. Minimum-distant scatterer offset distance from the direct path versus the total transmitter-to-receiver separation distance for three different excess delay times.

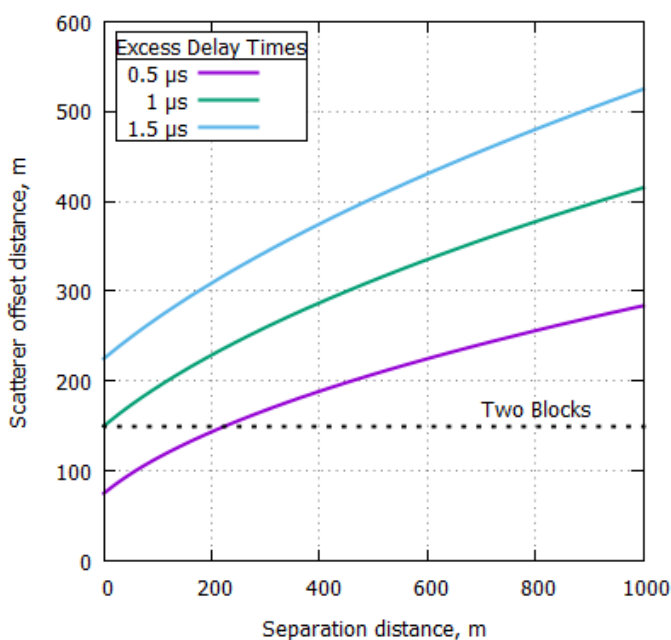


Figure 8 shows that (1) the $1 \mu\text{s}$ curve meets the “two-urban-block” criteria for all separation distances and (2) use of an excess delay-time criterion allows us to distinguish distant scatterers from canyon-mode propagation without having to explicitly specify the geometry for each case. Our distant-scatterer threshold of at least $1 \mu\text{s}$ excess delay ensures that they lie outside of the region where likely canyon-mode propagation paths exist.

The following example demonstrates our radio-geospatial analysis techniques and the inferences made possible through simultaneous analysis of channel sounding and geospatial data. In Figure 7, radio-geospatial analysis begins by correctly locating transmitter and receiver locations within the raster terrain and vector building representations of the environment. Using these items as inputs, we use custom software developed during this project to calculate a raster of bistatic delay times covering the area of interest. The shortest delay time corresponds to the most direct path (shown as a straight yellow line in Figure 7), while longer delays take on elliptical paths. These paths are shown as gray elliptical *bands* rather than lines in Figure 7 to more clearly show the impact of our finite channel-sounder bandwidth on our spatial resolution. The two tallest buildings in this scene are highlighted with red boxes and, because of their positions relative to the transmitter–receiver pair, fall on very different (relative to our $0.08 \mu\text{s}$ effective timing resolution) bistatic delay ellipses.

To interpret the PDP of Figure 7, we plot vertical lines at the geospatially predicted arrival times for both free-space propagation and any likely scatterers, such as particularly tall buildings, located within the scene. For this case, we found the following:

- The geospatially predicted direct path, indicated by the vertical green dashed line, agrees well with the first recorded signal arrival. This result suggests a propagation path following the yellow direct path over rooftops and diffracting or scattering down to ground level in the vicinity of the receiver, otherwise known as the *direct-rooftop propagation mode* (Laurila et al. 2002). Note that an LOS path would also arrive to coincide with the green line, but we would expect such an arrival to be dominant in terms of power.
- Arrivals within roughly $1 \mu\text{s}$ of the predicted free-space delay have typically traveled horizontally along one or more urban canyons, undergoing multiple reflections and sustaining losses due to vehicles, trees and

other common ground-level obstacles. This type of propagation, studied widely in the cellular literature and observable from 2 to 3 μs in the PDP of Figure 7, is known as the street-guided mode, or *canyon propagation mode* (Laurila et al. 2002).

- Beyond 1 μs of excess (meaning in excess of free space) delay time, canyon propagation becomes less and less viable as losses due to multiple reflection and ground-level obstacles rapidly accumulate. Significant arrivals in this time period likely come from high-rise buildings at a distance, or *distant scatterers* (Laurila et al. 2002), whose impact on the ground-to-ground channel depend on several factors: the strength of the incident signal upon the scatterer, the scatterer's diffuse radar scattering cross section (RCS), and the obstacles along the path from scatterer to receiver. A strong return from an isolated distant scatterer can be seen at 3.7 μs in the PDP of Figure 7 in excellent agreement with the predicted arrival time for a signal bistatically scattered from the Prudential Tower. The received power at the expected arrival time for 200 Clarendon at 5.35 μs is unremarkable, suggesting a significant difference in the scattering strength of these two large buildings.

As this example shows, radio geospatial analysis can provide important clues regarding the various propagation modes involved in a given radio link and plays a critical role in properly interpreting PDPs within their urban geospatial context.

3.1.2 Vertical components of bistatic range and delay

As discussed above, the total travel time of a radio signal is a function of the path taken in 3-D space; and with the extreme relief of urban environments, the vertical-component contributions (i.e., the time spent travelling to and from the upper levels of a building, in addition to the horizontal distance components) can become significant. Figure 9 shows the additional delay time (on a single leg of a two-leg bistatic path) associated with the vertical component of the signal path as a function of building height and the two-dimensional (2-D) horizontal distance between the radio terminal and the building of interest. The additional delays are most important for *radio terminals located close to large buildings*, a common scenario for essentially all of our measurements in Boston.

The vertical component for a single-leg delay is straightforward to calculate from

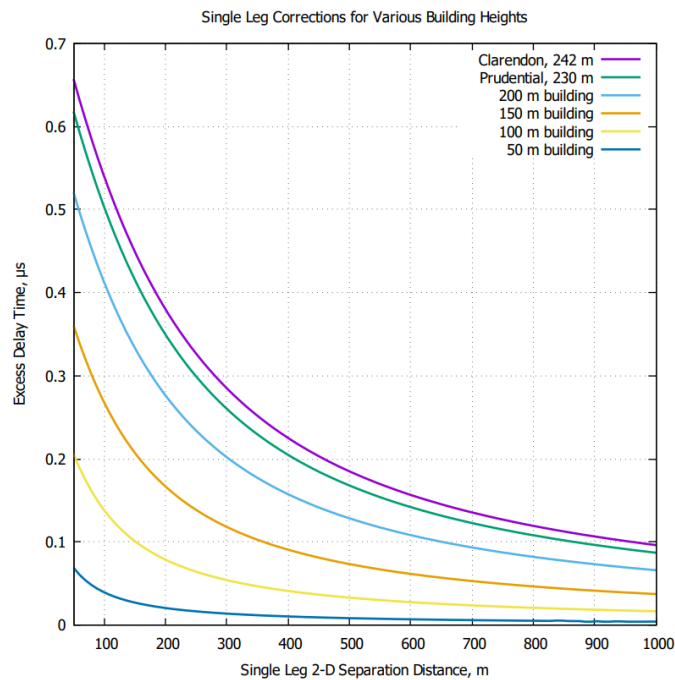
$$C(x, h) = \frac{(\sqrt{x^2 + h^2}) - x}{299.7 \text{ m}/\mu\text{s}},$$

where

- $C(x, h)$ = the vertical component of the bistatic delay time (μs),
 x = the horizontal separation distance between the radio terminal and the scatterer of interest (m),
 h = the elevation of the scatterer of interest relative to the radio terminal of interest (m);

and $299.7 \text{ m}/\mu\text{s}$ is the approximate speed of light in air. This relationship is plotted for selected values of h (including the specific heights of the Prudential Tower and 200 Clarendon) in Figure 9.

Figure 9. Delay-time corrections for 3-D paths in urban environments, as a function of horizontal separation distance and building height above ground level.



Correctly assessing the total bistatic delay for a given scatterer therefore involves

- obtaining the transmitter-to-scatterer and scatterer-to-receiver distances to determine the horizontal component of the bistatic delay, as discussed in the previous section;

- obtaining the elevation of the scatterer from the digital elevation model;
- using the relation plotted in Figure 9 to find the vertical component of the bistatic delay for both transmitter-to-scatterer and scatterer-to-receiver legs; and
- determining the overall bistatic delay by summing the horizontal and vertical components.

We note that using the maximum height of the scatterer will produce an upper bound on the vertical-component contribution to the bistatic delay. Given the limited temporal resolution of our sounding system, this simplification rarely presents problems in our interpretation of a given PDP.

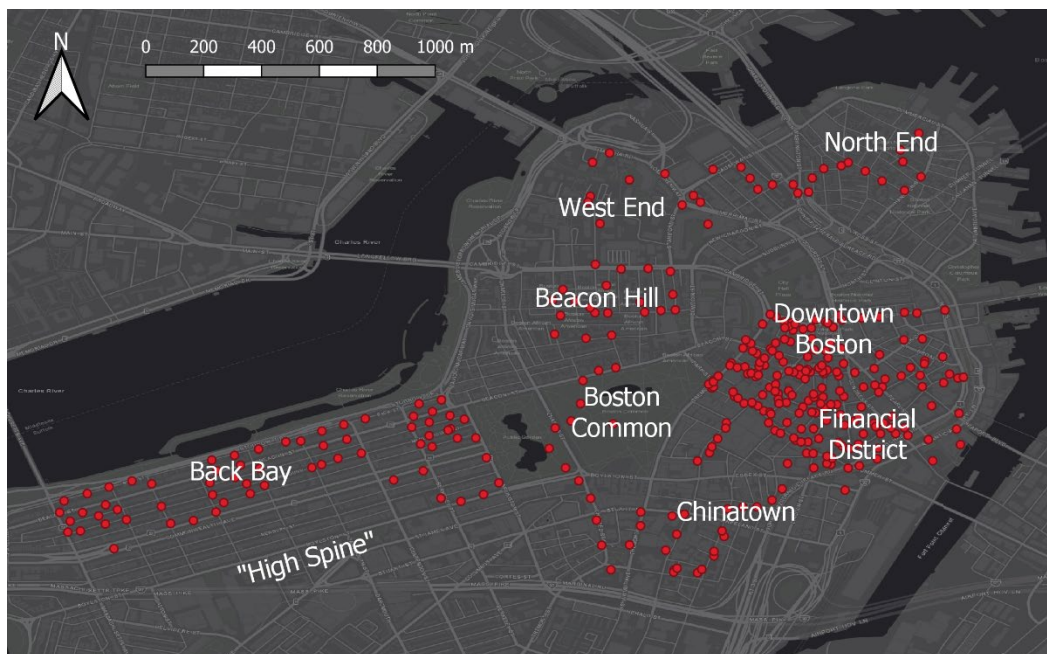
3.2 Channel sounding measurements

Sounding measurements occurred over four days in June 2018. Table 1 details each day, and Figure 10 provides an overall map of measurement locations. While most days were devoted to studies of a specific neighborhood, 7 June was used to circumnavigate Boston, investigating the impact of the urban core on adjacent intraneighborhood channels. All measurements were performed during normal working hours on weekdays to ensure that the collected data were representative of normal levels of noise, traffic, and human activity.

Table 1. Details of the Boston channel sounding campaign.

| Date | Neighborhood | Meas. Points | Comments |
|-------------|--|--------------|--|
| 5 June 2018 | Back Bay | 68 | One transmitter location on Commonwealth Ave. Data collection halted by rain. |
| 6 June 2018 | Downtown | 88 | Two transmitter locations: Dewey Square and Court Square. |
| 7 June 2018 | North End, West End, Beacon Hill, Boston Common, Chinatown, and Downtown | 98 | Circumnavigation of Boston with four transmitter locations: North End, West End, Beacon Hill, and Boston Common. |
| 8 June 2018 | Downtown | 92 | High-density survey of Downtown. One transmitter location at Post Office Square. |

Figure 10. Overview of Boston, Massachusetts, with relevant neighborhoods labeled and channel measurement sites indicated by *red points*.



3.2.1 Methods

Our sounding system was adapted for full-day urban use by mounting the equipment in handcarts and supplying the majority of the necessary power from a portable DC-to-AC* inverter drawing from a 108 amp-hour, 12V deep-cycle battery, also mounted in the cart. On a typical 8-hour measurement day, the system consumed 400 Wh of energy, roughly equivalent to running a desktop computer for one hour.

The receiving station was equipped with an RF switch and two identical, but orthogonally mounted, omnidirectional dipole antennae to allow for colocated measurement of both vertically and horizontally polarized signals. The transmitter used only a vertically polarized antenna as this is the most common polarization used in land mobile radio (Parsons 2000). Collection of both co- and cross-polarized measurements allows us to study the depolarization at a given measurement site. Our goal was to use depolarization as a tool to assess the effective electromagnetic roughness of the scatterers involved in hopes of differentiating certain building types from others.

* Direct-current-to-alternating-current

To avoid unnecessary noise and interference from cellular telephones or other radio communications devices, the transmitter and receiver teams used agreed upon times on the GPS clocks to synchronize measurements. Transmissions typically occurred every 2 minutes for a 30-second duration, providing sufficient time for the receiving station to move to a new location, obtain a GPS location fix, and perform two 5-second-long RF recordings, one for each polarization. As in Concord, forward transmit power was measured on a Bird 7020 Power Sensor and recorded on a Bird 5000-XT data logger. Geographical positions were recorded using a recreational-grade GPS receiver, so errors of 10 m or more were common due to GPS signal attenuation and multipath propagation within deep urban canyons (Paulson 2019). The transmit power was 9 W, comparable in power to commonly used handheld and man-pack radio systems. The antenna height of both the transmitter and receiver antennae was 2.5 m above ground level.

3.2.2 Depolarization of the urban radio-frequency channel

Electromagnetic waves are polarized, and this polarization is most often described in terms of the orientation of the electric field vector relative to some reference direction (Beckmann 1968). For terrestrial radio applications, the most commonly used reference is the plane of the ground, and thus waves with an electric field vector oriented normal to the ground are said to have a “vertical” polarization, while waves with electric fields parallel to the ground are said to be “horizontally” polarized (Degli-Esposti et al. 2011).

In attempting to capture both co- and cross-polarized measurements of the channel, we had hoped to explicitly test our second hypothesis that different buildings have measurably different impacts on the ground-to-ground channel based on their effective electromagnetic roughness. Rougher buildings should more effectively convert incident power of a given polarization into diffusely scattered (and thus largely depolarized) power (Degli-Esposti et al. 2007; Beckmann 1968) and thus more strongly influence the ground-to-ground channel.

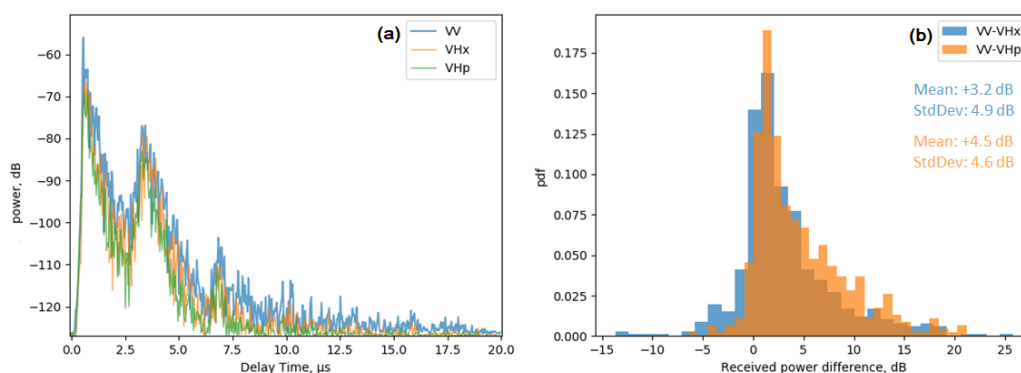
In practice, however, the observed depolarization was strong for the majority of our measured channels: copolarized channels were similar to cross-polarized channels in terms of their delay structure and relative power. Said another way, scatterers appearing in the copolarized measurements were always accompanied by scatterers present in the cross-polarized measurement. Figure 11a shows a measurement point on the western

side of the Back Bay neighborhood as an example of this widely observed channel behavior. The ratio of received vertically polarized power, P_{VV} , to horizontally polarized power, P_{VH} , is known as the cross-polarization discrimination ratio (XPD) and is expressed in decibels as

$$XPD = 10 \log_{10} \left(\frac{P_{VV}}{P_{VH}} \right).$$

Measurement locations where depolarization is strong (i.e., vertical and horizontal received powers are nearly equal) will yield XPDs close to 0 dB, while areas where the copolarized signal is more dominant might have XPDs somewhere between 8 and 10 dB (Degli-Esposti et al. 2011). Figure 11b shows a histogram of XPD values from the same location, indicating a value of about 3.3 dB for this location, which is typical of many of our measurements. Because this value is considerably lower than the values quoted above, it suggests that depolarization is stronger in a ground-to-ground channel compared to the elevated station-to-ground scenario measured and modeled by Degli-Esposti et al.

Figure 11. Comparison of collocated channel responses for three different polarizations. (a) Comparison of power delay profiles from a single location in Back Bay: vertically copolarized (VV), cross-polarized with the receiving antenna in cross-street orientation (VHx), and cross-polarized with the receiving antenna oriented parallel to the street (VHp). (b) Histograms of cross-polar discrimination (XPD) for the same location.



There are at least two interpretations of the similarities in the co- and cross-polarized PDPs and the corresponding low XPD values shown in Figure 11:

- Our hypothesis is correct to an extreme degree: if rough and therefore strongly depolarizing (Vitucci et al. 2012) scatterers are *the only ob-*

jects capable of influencing the ground-to-ground channel, then it follows that they will be the only scatterers to appear in a measurement of that channel, regardless of polarization.

- No polarization-preserving paths exist for the scatterer-to-receiver path. Given our low antenna heights, very few distant scatterers are *directly visible* to a ground-based receiver. This implies that signals reaching the receiver arrive via grazing paths over rooftops and then are directed downward either via diffraction at roof edges or by reflection from buildings opposite the direction of the scatterer (Ikegami and Yoshida 1980). These additional interactions in the vicinity of the receiver, especially those involving rooftop diffraction (Degli-Esposti et al. 2011), may be sufficient to increase the depolarization of the incoming signal.

Regardless of the depolarization mechanism, this finding places an important constraint on systems hoping to use polarization diversity to increase data rates or to combat fading in NLOS scenarios. Based on our data and comparison with Degli-Esposti et al. (2011), ground-to-ground channels appear to be more fully depolarized than the rooftop-to-ground channel, and thus attempts to exploit polarization diversity will be more challenging in the ground-to-ground scenario.

3.2.3 Radio-frequency channels in the urban core

Our work in Downtown Boston included several transmitter sites and many different receiving sites. The channels observed in Downtown all featured classic Saleh-Valenzuela tails (Saleh and Valenzuela 1987; Meijerink and Molisch 2014) and generally fell into two categories: those with and those without LOS to the transmitter.

Figure 12*a* and *b* shows examples of the two commonly observed types of channels, LOS and NLOS, drawn from the 8 June 2018 dataset. Figure 12*c* shows on the map the locations of the transmitter and two receiver points. As discussed in the previous section, very little difference exists between the co- and cross-polarized channels in either case.

Transmitter-to-receiver distances are about 200 and 250 m for the LOS and NLOS locations, respectively, and thus minimum absolute delays of 0.66 and 0.83 μs are expected, respectively. Table 2 lists relevant statistics for these channels, which indicate that, despite the similar transmitter-to-

receiver distances and their proximity within the same urban environment, the dominant propagation paths are quite different. While the peak power arrival for the LOS case is well aligned with the minimum expected time, peak power in the NLOS case lags the minimum by almost a full microsecond. The NLOS case also features larger path loss and RMS delay spread, indicating that in the absence of the direct path, a variety of other paths now come to dominate the channel. We use radio-geospatial analysis to infer the nature of these other paths.

Figure 12. Power delay profiles of co- (W) and cross-polarized (VHp) signals for (a) point M262, which has LOS, and (b) point M294, which does not have LOS to the transmitter. (c) Map showing locations of the receiving points M262 and M294 relative to the transmitter, PS-TX. Red lines indicate the 1 μ s contours of constant bistatic delay time for M294, evaluated for 2-D distances.

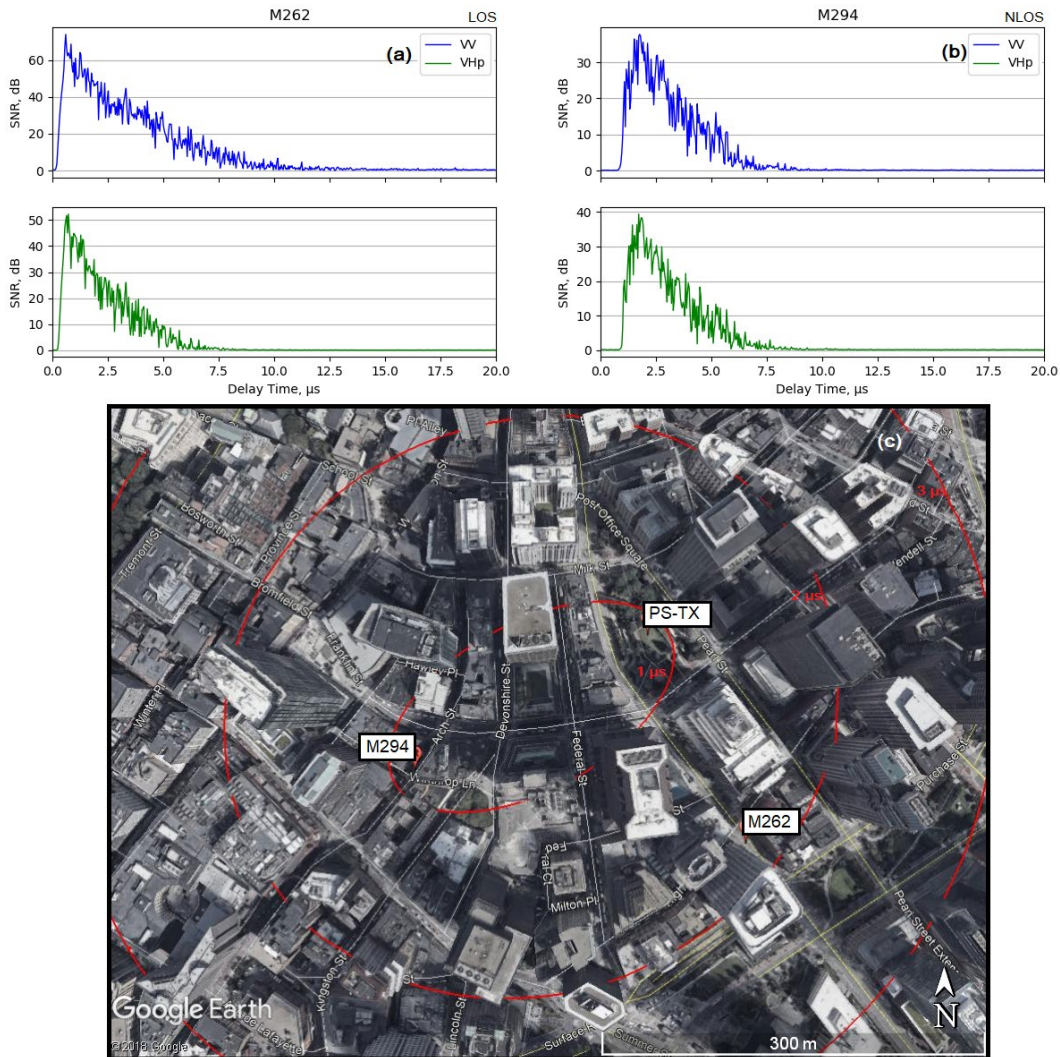


Table 2. Comparison of channel statistics for typical short-range LOS and NLOS channels in Downtown Boston.

| Site | Min. Abs. Delay (μs) | Peak Power Delay (μs) | Mean Delay (μs) | RMS Delay Spread (μs) | Path Loss (dB) |
|-------------|-----------------------------------|------------------------------------|------------------------------|------------------------------------|----------------|
| M262 (LOS) | 0.66 | 0.66 | 0.90 | 0.19 | 83.5 |
| M294 (NLOS) | 0.83 | 1.77 | 1.98 | 0.49 | 104.1 |

The map in Figure 12c has contours of constant bistatic delay time for measurement site M294 shown as red lines, indicating the time required for a signal to travel both the outbound (transmitter-to-scatterer) leg and the inbound (scatterer-to-receiver) leg, assuming single scattering. Inside the $2 \mu\text{s}$ line, we can see many tall buildings, all of which likely contribute something to the peak power; but it is difficult from this data to say if any building in particular is dominant. This is the usual case for urban core channels measured by a finite bandwidth sounding system using omnidirectional antennae: because the buildings are so close together, contributions of many individual scatterers can overlap and fall within the same delay-time bin, making it impossible to distinguish one scatterer from another (Salous 2013).

If we cannot resolve separate buildings in the Downtown neighborhood, what can be said about the paths composing the NLOS link to M294? The most direct urban canyon mode, assumed to be the most efficient *horizontal* conduit for RF power, follows Franklin and Arch Streets for a total distance of 330 m. This distance yields an absolute delay of $1.1 \mu\text{s}$, and we do observe an increase in received power at this point in the PDP of Figure 12b, but it falls short of the peak power by nearly 15 dB. The dominant paths, therefore, must lie outside of this direct canyon, leaving us with two possibilities. One is that longer, more tortuous urban canyon routes lead to the peak received power at $1.77 \mu\text{s}$, but this is unlikely due to the significant loss in signal power associated with multiple reflections and the lack of any obvious canyon route matching the observed delay. The curved street layout of Downtown Boston may act to limit the effectiveness of urban canyon modes compared with other, more rectilinear cities. The other possibility involves reflections from tall buildings directly illuminated by the transmitter.

Our transmitter site in Post Office Square is flanked by two 150 m tall buildings to the east, separated from the transmitter site by 65 and 100 m,

and separated from the receiver site by 310 and 330 m, yielding total bi-static delays, after applying the vertical-component corrections discussed in section 3.1.2, of 1.69 and 1.80 μs , respectively. These values agree well with the observed peak arrival time of 1.77 μs .

If this analysis is correct and scattering from high buildings (distant scatterers) is in fact the dominant propagation mode for NLOS ground-to-ground radio links in a dense urban core, then our results strongly support the argument that diffuse scattering is a critical part of the urban channel (Degli-Esposti and Bertoni 1999; Degli-Esposti 2001; Vitucci et al. 2012). Diffuse scattering appears to be important even if the second (scatterer-to-receiver) leg of the path suffers diffraction losses in passing from adjacent rooftops down to the receiver at street level. In the following section, we investigate channels in regions *adjacent to an urban core* and find that high buildings and the diffuse scattering they provide continue to play an important role in the ground-to-ground RF channel.

3.2.4 Radio-frequency channels adjacent to an urban core

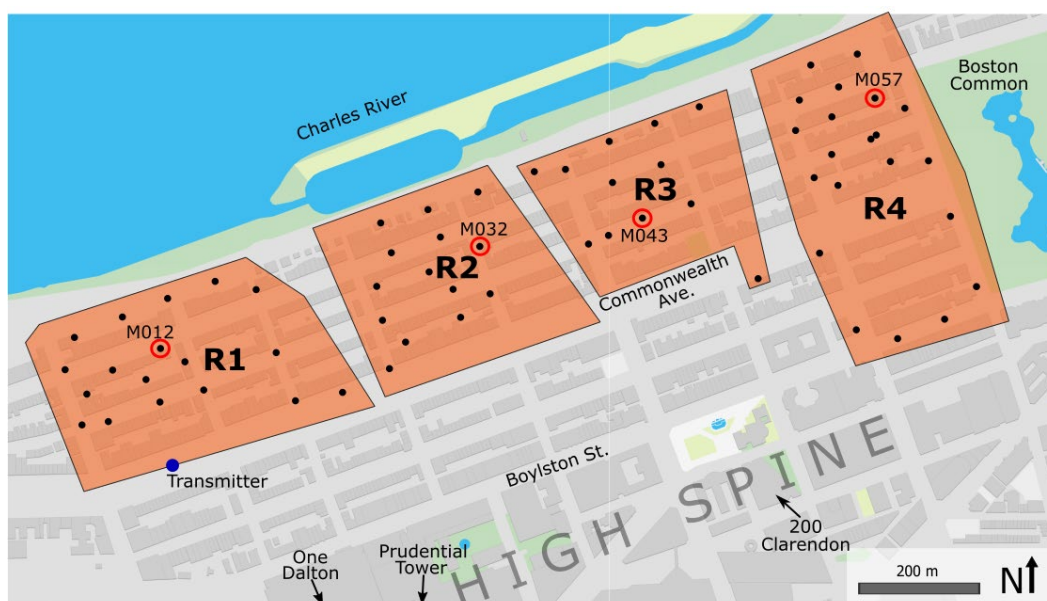
In this section, we investigate the structure of RF channels in the Back Bay neighborhood. Back Bay consists primarily of two to four story residential brick buildings arranged on a rectangular street plan; the cover photo of this report shows such buildings in the background. This region is bounded to the north by the Charles River; to the east by Boston Common; and to the south by the High Spine of Boston, a series of tall buildings running approximately 1 km along the length of Boylston Street. The High Spine includes 200 Clarendon Street (241 m), the Prudential Tower (228 m), and One Dalton Street (226 m final height), the three tallest buildings in New England. One Dalton Street was under construction at the time of these measurements on 5 June 2018. The building was roughly half of its final height, and no building cladding had been installed. Despite several large cranes present at the construction site, this incomplete building did not dominate any of the RF channels of Back Bay.

Figure 13 gives an overview of our work in the Back Bay neighborhood. Our fixed, vertically polarized transmitter was set up at the western end of Commonwealth Ave., a long east–west running greenspace approximately 60 m wide. The eastern end of Commonwealth Ave. terminates in the Boston Common, an open park covering 0.33 km². The upper portions of all three of the previously mentioned tall buildings were visible from the

transmitter point, though for One Dalton Street, this was primarily in the form of construction cranes as mentioned earlier.

The receiving team traveled over 6.2 km, covering an area of 0.5 km² in the Back Bay neighborhood, capturing the RF channel in a variety of locations, including streets, narrow alleyways, and open spaces. Both co- and cross-polarized measurements were conducted at each point, with results similar to those discussed in section 3.2.2. Because the streets and alleyways traversed by the receiving team were narrow and generally oriented southwest–northeast, the receiving antenna rarely had a direct view of any of the major buildings along the High Spine.

Figure 13. Map of the Back Bay neighborhood, showing the location of the transmitter site, study regions R1 through R4, and the three highest buildings along the High Spine. *Dots* indicate channel measurement points; *red-circled dots* are representative channels discussed in the text.

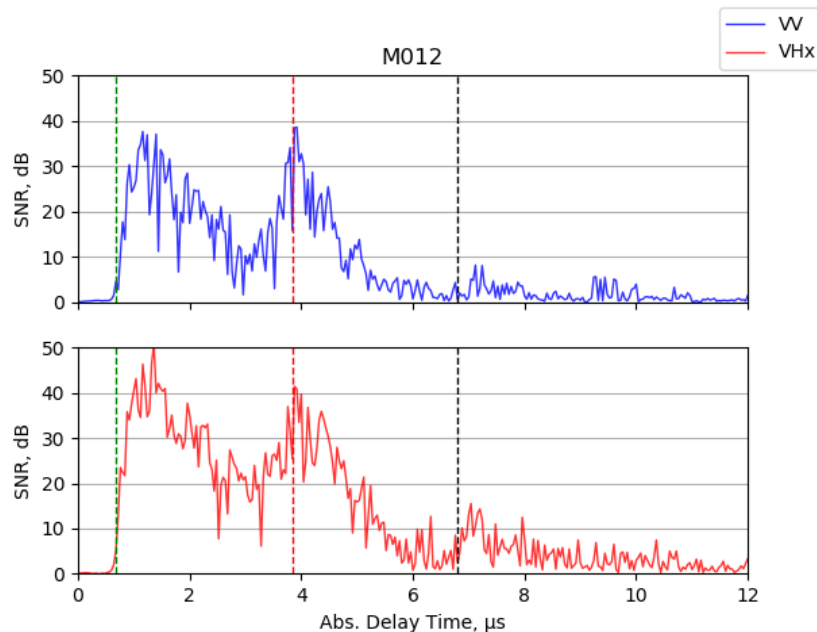


To summarize a large amount of data, we will present channels chosen from four representative sections of the Back Bay neighborhood. Because of the large and widely spaced high-rise buildings along the High Spine, these scatterers are often resolvable by our sounding system; and thus we can productively apply geospatial analyses to learn more about the impact of specific scatterers on the channel. Note that in study region R4, reflections from Downtown Boston (not shown on Figure 13) were frequently observed, though the individual scatterers within the urban core are too dense to be resolved.

3.2.4.1 Back Bay study region R1

Study region R1 is closest to the transmitter point, with transmitter-to-receiver separation distances ranging from 120 to 330 m. Because of the relatively short distances and simple urban canyon geometries, channels in this area typically feature strong arrivals via urban canyon modes as well as those from distant scatterers. Point M012, with a 207 m transmitter-to-receiver distance, lies roughly in the center of the study area and is representative of these channels. The co- and cross-polarized PDPs, shown in Figure 14, are generally similar: both lack an LOS arrival, have canyon propagation mode arrivals (1 to 2 μs absolute delay time), and also have arrivals from distant scatterers along the High Spine (3.7 to 4.3 μs). The expected arrival from the Prudential Tower (red vertical line) is equal in power to the canyon modes, while the expected arrival from 200 Clarendon (black vertical line) is weak, if present at all. As a consequence of the significant power arriving via distant scatterers, the RMS delay spread for this channel is relatively large at 1.03 μs .

Figure 14. Co- (VV) and cross-polarized (VHx) power delay profiles for point M012 in Back Bay study region R1. The *green vertical line* indicates the free-space arrival time, the *red vertical line* is the expected arrival from the Prudential Tower, and the *black vertical line* is the expected arrival from 200 Clarendon.



There are three results worthy of discussion:

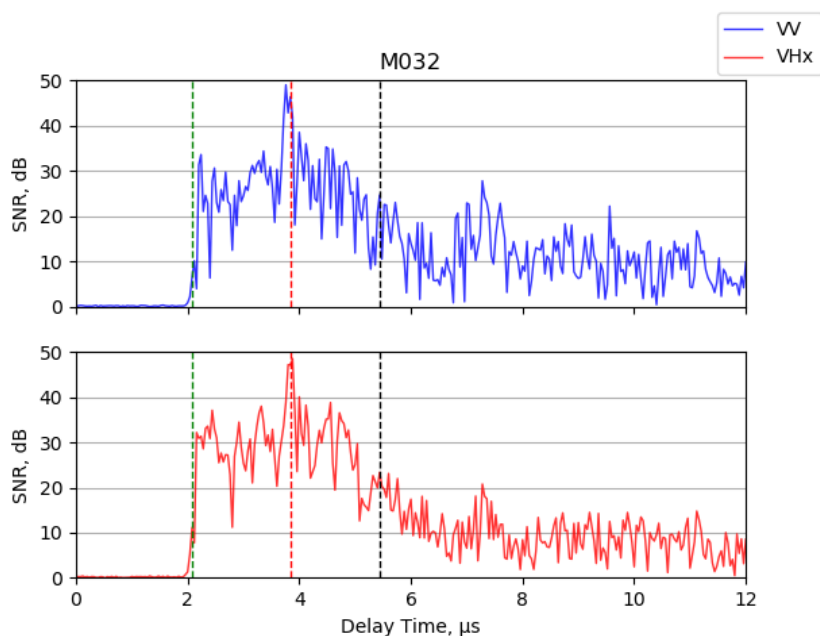
- First, the most direct, over-rooftop path is negligible compared to other propagation modes, even though the separation distances are relatively small in the R1 study region.
- Second, the distant-scatterer contribution to the received signal is comparable to that of the canyon mode, even though the distant scatterer is only partially visible to the transmitter and completely obscured by nearby buildings at the receiver. Distant scattering, primarily from the Prudential Tower, made important contributions even at measurement points along the far north section of R1, where there are no buildings lying to the north of the receiver to capture and reflect the signal down to ground level.
- Third, the lack of any identifiable arrival from 200 Clarendon, the tallest building in New England and well isolated from other structures of similar size, is a remarkable result. Despite its size and proximity, it is unimportant to this ground-to-ground channel, and we discuss this discrepancy in more detail in section 4.3.6.

3.2.4.2 Back Bay study region R2

Study region R2 has transmitter-to-receiver separation distances ranging from 395 to 685 m. Channels in this study region are influenced (and often dominated) by distant reflectors and are generally similar to those in R1. Arrivals via canyon propagation modes tend to be weaker due to the longer distances and increased numbers of reflections required to complete the radio link.

The channel measured at point MO32, shown in Figure 15, exhibits this behavior. Here we have a relatively strong “direct” arrival followed by a dominant scattered arrival from the Prudential Tower at $3.9 \mu\text{s}$ and again no detectable scattering from 200 Clarendon. To so closely match the free-space arrival time, the direct arrival likely travels over rooftops and then diffracts (or is reflected by buildings on the opposite side of the street at the receiver) down to the street level. Bertoni (2000) and Ikegami and Yoshida (1980) discussed this rooftop propagation mode.

Figure 15. Co- (VV) and cross-polarized (VHx) power delay profiles for point M032 in Back Bay study region R2. *Green, red, and black vertical lines* indicate expected free-space, Prudential Tower, and 200 Clarendon arrival times, respectively.

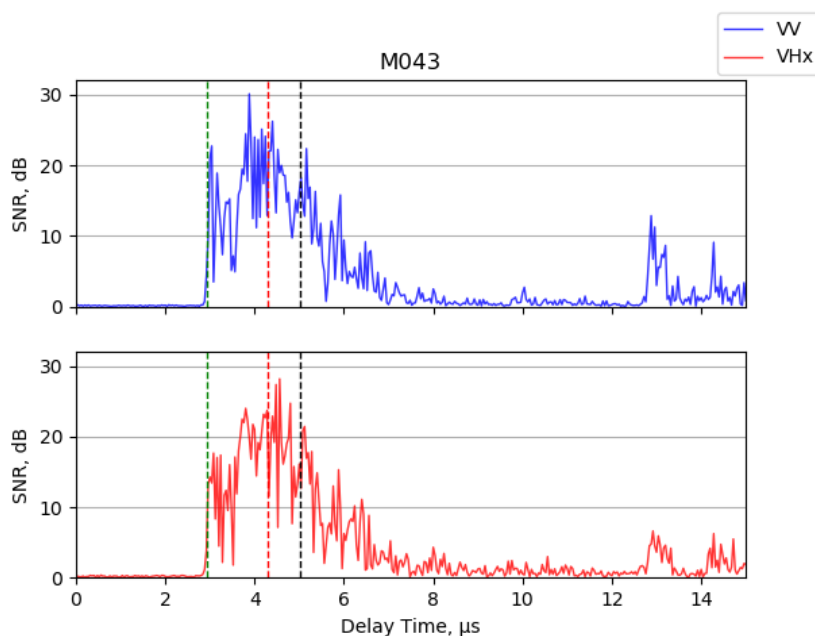


3.2.4.3 Back Bay study region R3

Study region R3 has transmitter-to-receiver separation distances ranging from 775 to 1060 m. Channels in this study region, like those in R2, commonly feature rooftop-mode arrivals at the expected free-space arrival time. In R3, distant reflectors always dominate the channel (typical RMS delay spreads are 2.8 μs); however, it is not always straightforward to assign a scatterer observed in the PDP to a given structure.

Our typical measurement for R3 is point M043 (see Figure 16), which shows a rooftop-mode arrival followed by a wide swath of distant scatterers from 3.5 to 5.5 μs . Expected arrival times for the Prudential Tower and 200 Clarendon do not convincingly align with any obvious peaks in received power; however, the overall arrival window is consistent with distant scatterers along the High Spine. The R3 study area is different from the other areas in that scattering from Downtown Boston now begins to weakly impact the channel, starting at 12.8 μs with scattering clearly identifiable from One Beacon St., followed by additional returns from other structures deeper into the urban core. All measurements taken in R3 feature some influence from Downtown Boston.

Figure 16. Co- (VV) and cross-polarized (VHx) power delay profiles for point M043 in Back Bay study region R3. *Green, red, and black vertical lines* indicate expected free-space, the Prudential Tower, and 200 Clarendon arrival times, respectively. Weak returns from Downtown Boston can be observed starting at 12.8 μ s.

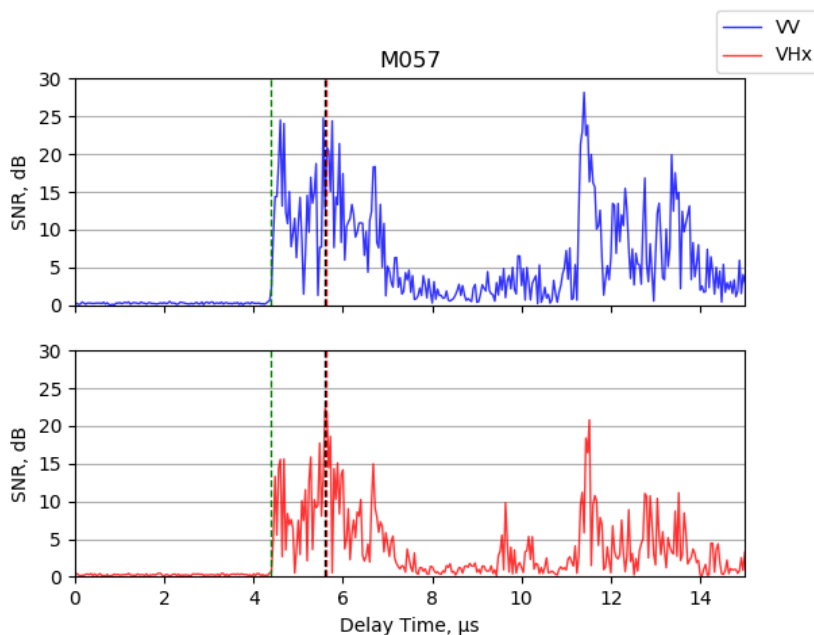


3.2.4.4 Back Bay study region R4

Study region R4 is adjacent to Boston Common and has separation distances ranging from 1150 to 1360 m. At this distance, both canyon propagation modes and rooftop modes are still present, though the channel is dominated by distant scatterers. Typical RMS delay spreads are around 3 μ s, though this varies widely depending on the strength of rooftop and canyon modes relative to the now considerable power scattered from Downtown Boston, as seen below in Figure 17.

Our example channel (shown in Figure 17) is from point M057, near the eastern edge of R4. This is a complicated channel with multiple propagation modes all received at comparable power levels. This particular geometry is unique in that scattered signals from both the Prudential Tower and 200 Clarendon are expected to arrive at 5.6 μ s; and while we do observe a peak in received power at this point, it is impossible to assess the relative importance of each building to this arrival.

Figure 17. Co- (VV) and cross-polarized (VHx) power delay profiles for point M057 in Back Bay study region R4. The *green vertical line* indicates expected free-space arrival time. The Prudential Tower and 200 Clarendon arrival times (*red and black vertical lines*) overlap at $5.6 \mu\text{s}$ for this geometry. Strong returns from Downtown Boston start at $11.3 \mu\text{s}$.



3.3 Summary

We obtained channel sounding measurements in a wide variety of urban areas in and around Boston. These measurements were interpreted with the aid of geospatial analysis tools and algorithms specifically designed by the CRREL Radio Science Laboratory over the course of this project.

We observed significant differences between observations made within the urban core versus those made in neighborhoods adjacent to the urban core. Within the urban core, we found that while canyon propagation modes play a role, the NLOS channel is frequently dominated by scattering from buildings directly illuminated by the transmitter and potentially even from those that are indirectly illuminated. Channels measured in the urban core, beyond the obvious LOS vs. NLOS differences, were generally similar in appearance as the bandwidth of our sounding system was too low to resolve the many scatterers present within the urban core.

Outside of the urban core, distant scatterers tend to dominate the channel in all but the shortest range links, even when those scatterers are occluded by buildings in the vicinity of the transmitter and receiver. The Back Bay

neighborhood of Boston was a particularly good laboratory for our purposes as there are several tall and geographically isolated buildings adjacent to our area of study, providing scatterers spatially resolvable by our sounding system. Channels within Back Bay varied not only as a function of transmitter-to-receiver separation distance but also as a function of proximity to adjacent scatterers. For example, in the study region closest to the transmitter (R1), we found that all three propagation modes (rooftop, canyon, and distant scatterers from the High Spine) were important. In the most distant region (R4), distant scatterers were dominant and mainly found to lie within Downtown Boston.

Our results from Back Bay (and other neighborhoods not covered in this section) describing the importance of distant scatterers are, however, contrary to those of Laurila et al. (2002), who reported the dominance of canyon-mode propagation for both ground-to-ground and rooftop-to-ground scenarios. Because the studied frequencies are significantly higher in the Laurila et al. study (2154 MHz vs. our work at 437 MHz) and transmitter-to-receiver separation distances were limited (less than 500 m vs. our work with many links over 1 km), the different conclusions are not surprising. Higher frequencies typically suffer greater diffraction losses (Bertoni 2000), and thus propagation paths involving rooftop diffraction (i.e., rooftop and distant-scatterer modes) are bound to be significantly weaker in Laurila et al.'s work as compared to our work in Boston.

The frequency dependence of diffraction phenomena therefore appears to be an important control on the structure of urban channels, the related data capacity of those channels, and the effective range of NLOS links in urban terrain. In the next section, we will investigate several modeling approaches that ignore this frequency dependence (relying instead on high frequency, i.e., optical, approximations) and find that their results compare poorly against the measurements presented above.

4 Radio-Frequency Channel Modeling

The overall goal of RF channel modeling within this project was to model the idealized case where all scatterers have the same *normalized RCS*, defined as the RCS divided by the projected area of the scatterer (Long 2001). Comparing this idealized channel with measured channels allows us to analyze the differences in scattering cross sections between different buildings, thus enabling us to test our second hypothesis—that not all buildings effect the channel equally because of their material and structural differences. Existing channel models proved to be inadequate when compared with measured data.

Following (Turin et al. 1972a), an RF channel can be modeled mathematically as a linear filter by accounting for the amplitude, delay, and phase change associated with each of the k paths composing a multipath radio link. The received time domain signal can be written as $\text{Re}\{\rho(t) e^{i\omega_0 t}\}$, where the influence of the channel on the received signal is captured by

$$\rho(t) = \sum_{k=0}^{\infty} a_k s(t - t_k) e^{i\theta_k} + n(t),$$

where

- t = time,
- a_k = the amplitude of the k^{th} path,
- t_k = the delay time of the k^{th} path,
- θ_k = the relative phase of the k^{th} path,
- $s(t)$ = a complex-valued low-pass waveform sent from the transmitter, and
- $n(t)$ = the complex-valued low-pass additive noise.

While the relative phase of the various paths is expected to be randomly and uniformly distributed over $[0, 2\pi)$, the amplitudes and delay times of the paths depend intimately on the propagation environment. Path amplitudes will depend on the path length, the RCS of the structure involved, and the influence of various propagation loss mechanisms. The delay time for single-scattered paths is controlled by bistatic path geometry, but multiple scattered paths have delay times that are much more difficult to assess. There are, therefore, three main parameters to be determined or estimated in RF channel modeling: geometry, loss mechanisms, and RCS.

RF channel modeling can take several different forms (Almers et al. 2007), but the *deterministic physical* modeling approach taken in this project was driven by the need for direct comparison against geospatially specific channel measurement data: for our purposes, the virtual and actual environments needed to match closely. Such an approach requires detailed geospatial data (on the order of a few wavelengths for the frequency of interest) to properly simulate the terrain, the built environment, and the radio link geometry. For the modeling work described in this report, we primarily used COLLADA (COLLABorative Design Activity) and Esri Multipatch Shapefiles, which are detailed, 3-D representations of the city and are freely available from the Boston Planning and Development Authority.

The following sections describe three different deterministic physical modeling approaches to understanding the urban channel. Section 4.1 describes the use of commercial ray-tracing software specifically designed for radio propagation modeling. Section 4.2 describes the use of an optical ray-tracing technique that attempts to find and quantify on urban structures the co-visible areas contributing to the RF channel. Finally, section 4.3 describes the Building Raster Urban Channel Estimator (BRUCE), a radio-geospatial model developed within this project to explicitly account for incident RF power on occluded buildings when estimating the urban channel.

4.1 Radio-frequency channel modeling with ray tracing

Our initial attempt at modeling the RF channels of Boston used the Wireless InSite commercial ray-tracing software produced by Remcom, Inc. The software takes as input a full 3-D model of the urban environment along with transmitter and receiver locations within that environment. The software uses ray tracing to identify and quantify the RF power delivered over the various paths connecting the transmitter and receiver.

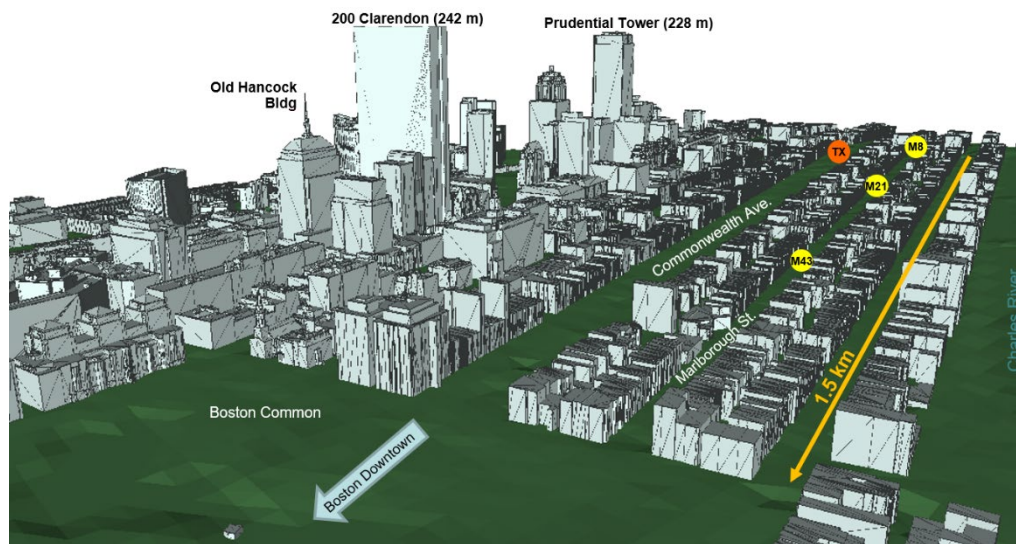
Additional inputs include radio-system parameters, such as frequency, bandwidth, antenna gain and height, and ray-tracing parameters, such as number of allowed reflections and diffractions before the propagation of a given ray is terminated. Table 3 lists the modeling parameters for all of the ray-tracing results shown in this section.

We will examine three representative locations within the Back Bay neighborhood, shown in Figure 18, and compare ray-tracing results with actual channel measurements performed in the same locations.

Table 3. Ray-tracing model parameters.

| Parameter | Value | Parameter | Value |
|--------------------------------|---|---------------------------------|--|
| Antenna type | Half-wave dipole | Transmitter antenna height | 10 m |
| Receiver antenna height | 2.5 m | Transmitter frequency | 437 MHz |
| Receiver collection radius | 9 m | Transmitted waveform | 40 ns Gaussian pulse |
| Building material | Concrete: $\epsilon_r=15.0$, $\sigma = 0.015$ S/m | Ground material | Wet earth: $\epsilon_r=25.0$, $\sigma = 0.015$ S/m |
| Max. number of ray reflections | 8 | Max. number of ray diffractions | 3 |
| Ray angular spacing | 0.25° | Max. number of ray interactions | 16 |

Figure 18. Virtual model used for ray-tracing studies of ground-to-ground channels in Back Bay, Boston. TX is the transmitter, and receiver points are indicated by labeled yellow circles. Not shown but present in the model is Downtown Boston, which lies across Boston Common in the direction indicated by the blue arrow.

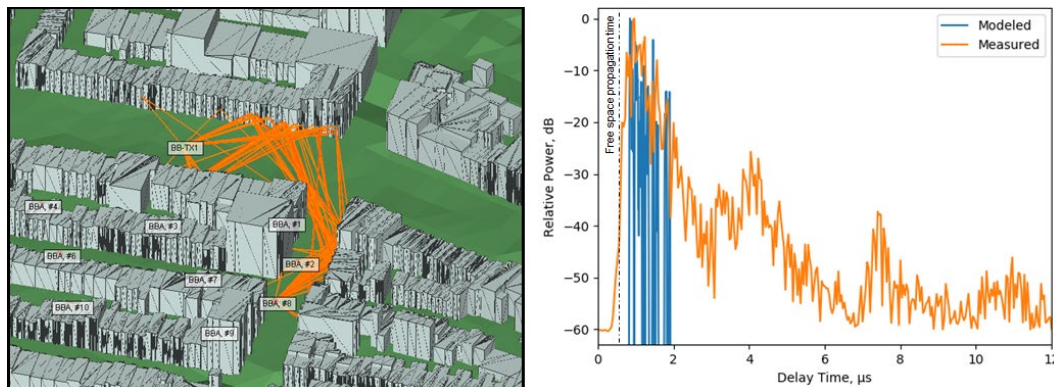


4.1.1 Short range, one turn (M8)

The transmitter and receiver are separated by a direct-path distance of 155 m. Given this short distance, the expected propagation modes are over-rooftop and canyon propagation through a single 90° turn from Commonwealth Ave. onto Massachusetts Ave. The rays found by the ray-tracing technique lie mainly within the urban canyon connecting the transmitter to the receiver, leading to the modeled PDP shown in Figure 19. This PDP agrees nicely with the measured channel for “important paths,” gen-

erally defined as those within 15 dB of the peak power (International Telecommunications Union 2019). We note that the modeled PDP does not indicate any contributions from rooftop or distant-scatterer propagation modes, while the measured channel shows that these modes are present but not necessarily important.

Figure 19. Modeled rays (*left*) and both modeled (*blue*) and measured (*orange*) power delay profiles (*right*) for receiver point M8.

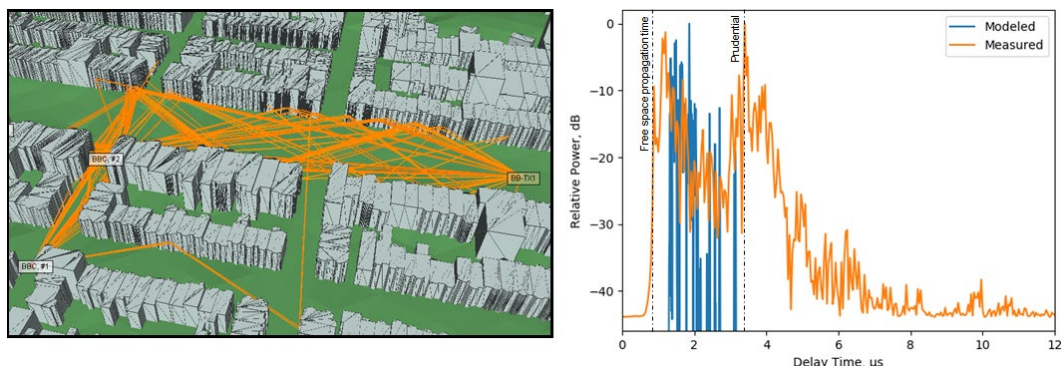


4.1.2 Medium range, one turn (M21)

In this case, the transmitter-to-receiver distance is 280 m, again with a one-turn urban canyon geometry (Commonwealth Ave. onto Gloucester St.). With the additional range and potential for losses along canyon paths, we expect that all three propagation modes (rooftop, canyon, and distant scatterer) could be important. The measured PDP in Figure 20 shows that this is the case, while the modeled rays and modeled PDP suggest that only canyon modes are relevant, thereby significantly underestimating the complexity of this NLOS channel.

It appears that the ray-tracing model deems only canyon-mode rays to be powerful enough to make important contributions to this channel. On our first modeling attempts, we believed that the cause was the low transmit-antenna height of 2.5 m: roof edge diffraction losses were too great to allow these rays to contribute. We thereafter (see Table 3) set the antenna height to be four times higher (10 m) than the actual height in an attempt to enable rooftop and distant-scatterer ray interactions. While this height is roughly at rooftop level for this neighborhood, the modeled contributions from rooftop and distant-scatterer modes were still negligible.

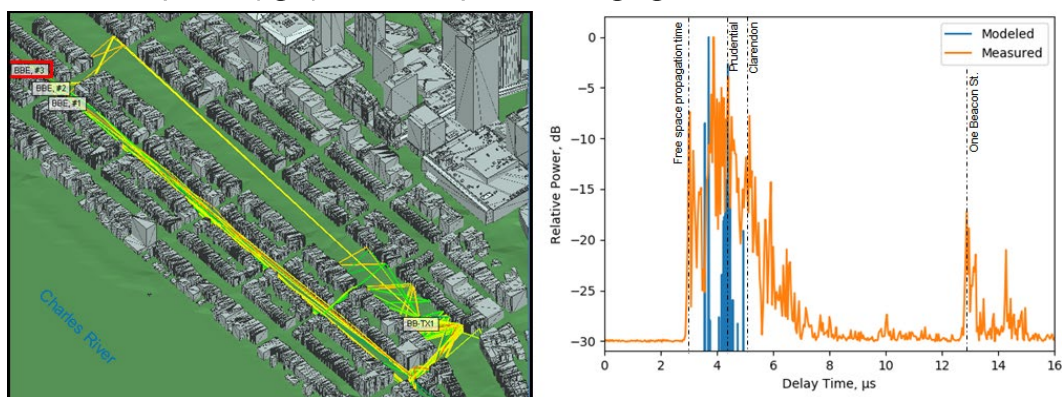
Figure 20. Modeled rays (*left*) and both modeled (*blue*) and measured (*orange*) power delay profiles (*right*) for receiver point M21.



4.1.3 Long range, two turn (M43)

The transmitter-to-receiver distance is 910 m in this case, with a two-turn urban canyon geometry (Commonwealth Ave. to Marlborough St. via either Dartmouth or Clarendon Streets). Given the longer range (and thus more opportunities for losses) involved, we would expect that canyon-mode propagation would be considerably weaker than other modes. The measured results in Figure 21 show that this is the case. The modeled channel consists of two sets of canyon-mode arrivals: one centered around 3.7 μs associated with Commonwealth Ave. and another centered at 4.3 μs associated with the many rays traversing Marlborough St., on which the receiver lies. The Marlborough St. arrivals align with the expected arrival time for signals scattered from the Prudential Tower, so the model-measurement agreement at the 4.3 μs point is a fluke of geometry.

Figure 21. Modeled rays (*left*) and both modeled (*blue*) and measured (*orange*) power delay profiles (*right*) for receiver point M43, highlighted with the red box.



4.1.4 Summary of ray-tracing results

The computational cost of ray tracing is often significant (Almers et al. 2007), and our work here is no exception: the model calculations presented here required several hours to process urban geometry to find faces and edges, run the ray-tracing algorithm, and produce a PDP for a single transmitter–receiver pair.

For simple, short-range urban links, ray tracing appears to nicely capture the time-dispersion effects associated with canyon propagation modes. Despite using an artificially elevated transmitter antenna to improve the chances of observing rooftop and distant scatterer modes within the model, such modes were generally of no importance to the channel.

While it is difficult to explain the absence of the rooftop mode in the modeled results, it is important to point out that the model does not explicitly account for diffuse scattering: it considers only specular reflections and diffractions from building edges. This poses a substantial limit on the applicability of such models to the ground-to-ground channel, as this approach essentially limits the effective area of distant buildings to their horizontal and vertical edges, thereby greatly reducing their potential importance to the channel. Our measurements suggest otherwise, and we believe that the lack of a diffuse scattering mechanism explains the significant differences between model and measurement. Without a physical mechanism within the model to distribute RF power back down towards the ground, most upward directed rays are specularly reflected and lost to the virtual sky, leaving only canyon-mode rays to describe the channel.

If, as the above results suggest, traditional ray tracing fails to adequately account for areas on distant scatterers leading to diffuse scatter, then perhaps locating and quantifying these covisible areas directly would help improve agreement between model and measurement. The next section discusses our attempt to accomplish this using optical covisibility analysis.

4.2 Urban covisibility studies with optical ray tracing

The approach described in this section sought to specifically identify and quantify the areas of urban structures that were simultaneously visible (covisible) to both transmitter and receiver. If the location and magnitude of these areas can be found, then it becomes possible to estimate the impact of distant scatterers on the channel on the basis of their covisible area. The

methods used in this section are based on optical ray tracing and will necessarily be a lower estimated bound on the area because optical (in the sense of being a high-frequency approximation for radio waves) rays ignore the often significant diffraction effects associated with radio waves. Even using this optical approximation, determining the areas of interest within an urban environment is not trivial, however.

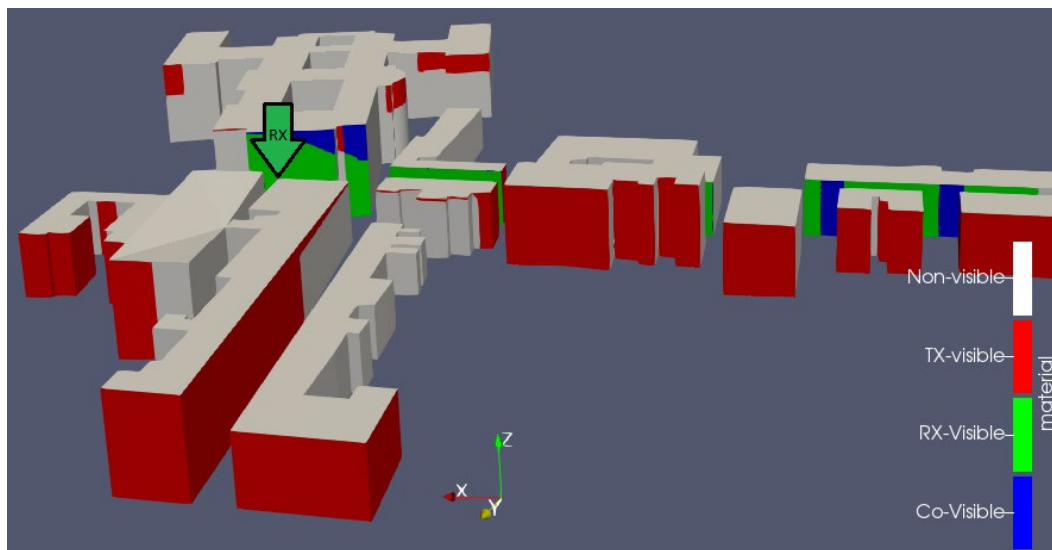
Viewshed analysis is a common geospatial operation (Izraelevitz 2003; Cuckovic 2016) that takes in a 2-D raster representation of terrain elevations and determines which parts of the terrain of interest are visible from a given point. The resulting viewshed is typically output as a raster as well, with visible pixels assigned the value “1” and nonvisible pixels assigned the value “0.” If surface slopes are reasonably small, the viewshed operation can be used to estimate the area viewed from a given point.

However, in terrain where surface slopes are very high (e.g., ground-to-building transitions in urban environments), it becomes impossible to determine the viewed area using the viewshed alone. Especially for ground-based observers where the majority of viewable areas lie on the vertical faces of buildings, we require more sophisticated methods to find viewable area. For this work, we performed the visibility analysis using the RayCaster software developed by Alex Castillo of the ERDC Geotechnical and Structures Laboratory. This software, like Wireless InSite, ingests a full 3-D representation of the urban environment and the locations of two points (transmitter and receiver) within that environment and then assesses the visibility of surfaces within the scene through ray tracing. Unlike Wireless InSite, RayCaster does not analyze for reflection or diffraction but instead uses straight, single rays to evaluate visibility in a 3-D environment.

RayCaster uses 3-D building models in the form of 2DM files, a commonly used digital exchange format for finite element meshes. These files were derived from the Esri multipatch Shapefiles obtained from the Boston Planning and Development Authority. We developed custom software to convert the multipatch Shapefiles into 2DM files. The main inputs into this code are the coordinates of the transmitter and receiver plus a list of georeferenced 2DM files composing the buildings in the scene. The virtual buildings then go through several stages of refinement where the surfaces are subdivided into small triangular patches, and the visibility of each of those patches is evaluated through optical ray tracing from the point of interest.

Visibility is evaluated for both transmitter and receiver points, and then the covisible areas are determined by performing a logical AND operation on the transmitter and receiver visibility fields. The final output of the code is a list of building faces (each with a particular location in space) and the covisible area associated with it. Figure 22 shows an example covisibility analysis.

Figure 22. Optical covisibility results from the RayCaster software for a small-scale urban environment. The ground-level transmitter (*TX*) is distant in the +Y direction, while the receiver (*RX*) lies at ground level between two buildings, as the *green arrow* indicates. The visibility state of various surfaces is indicated by color.



The overall goal of this analysis was to assess what Wireless InSite could not: the influence of distant scatterers on the RF channel. We thought that optical ray tracing, widely used in computer graphics rendering processes, could provide a rapid estimate of the relative importance of various distant scatterers to the radio channel.

Unfortunately, this approach required significant amounts of geospatial preprocessing, followed by hours of computing time, and in the end did not reproduce the rich channel structure observed via measurement. The covisible areas, when they existed, were quite small and generally did not exist for medium to long-range urban links. In short, the optical covisibility analysis did not identify the major scatterers observed in our measurements and, therefore, could not estimate the magnitude of area involved.

Given the results of this section (RayCaster) and the section prior (Wireless InSite), it became clear that the models used were not properly capturing the radio illumination of buildings from ground-based transmitters. The following section describes our attempts to build on our lessons learned from ray tracing and explicitly include diffraction effects on building illumination.

4.3 Building Raster Urban Channel Estimator (BRUCE): geospatial radio-frequency channel modeling via incident power profiles

The approach described in this section seeks to explicitly include diffraction effects such that *all* power incident on a given scatterer is properly accounted for, even when that scatterer is occluded, or not fully visible from the transmitter or receiver points. Such an accounting requires analysis of the full vertical profile of the power incident upon a given scatterer, which in turn depends on the size and location of obstacles lying on the transmitter-to-scatterer path. The potential impact of a given scatterer on the channel, therefore, depends on both the total incident power and the location of the scatterer relative to the transmitter–receiver pair. Based on our understanding of the current literature and modeling efforts, the analyses and codes developed in this section represent a new contribution to the field of channel modeling.

4.3.1 Vertical profiles of radio-frequency power incident on buildings

We begin by evaluating the vertical profile of the RF power incident on an occluded scatterer in an urban environment. The vertical profile of incident power is largely controlled by diffraction over obstacles lying along the transmitter-to-scatterer path. We make two simplifying assumptions in assessing the vertical incident power profile:

- Only the two most important obstacles lying in the transmitter-to-scatterer path are considered in determining the incident power profile on the building face of interest: the *controlling* and *secondary* obstacles, which are described below.
- The diffraction effects associated with the controlling obstacle can be modeled with simple knife-edge diffraction (KED).

The obstacle with the largest slope angle relative to horizontal (as observed from the transmitter) is assumed to be the dominant control on the incident power profile and is therefore called the *controlling obstacle*. This is

a significant assumption (Deygout 1966), and the controlling obstacle will almost always be a building immediately adjacent to the transmitter site. The *secondary obstacle* has the second-largest slope angle on the path between the transmitter and the building face of interest and captures shadowing of the tallest obstacle lying between the controlling obstacle and the building face of interest.

KED is widely used (Durgin 2009) due to its simple geometric interpretation and its tractable mathematical form. Diffraction losses for the KED approximation depend only on the diffraction parameter:

$$v = h \sqrt{\frac{2}{\lambda} \left(\frac{1}{d_1} + \frac{1}{d_2} \right)},$$

where

- h = the height of the top of the obstacle above (or below) a straight line connecting the two ends of the radio path (if the obstacle top is below this line, then $h < 0$),
- λ = the wavelength of the radiation,
- d_1 = the distance between the transmitter and the top of the obstacle,
- d_2 = the distance between the top of the obstacle and the receiver.

With the diffraction parameter obtainable from knowledge of the wavelength and the overall geometry, the exact KED diffraction loss in decibels is expressed as

$$J_{exact}(v) = -20 \log_{10} \left(\frac{1}{2} \sqrt{[1 - C(v) - S(v)]^2 + [C(v) - S(v)]^2} \right),$$

where

- $C(v)$ = the Fresnel cosine integral evaluated at v , $\int_0^v \cos(t^2) dt$, and
- $S(v)$ = the Fresnel sine integral evaluated at v , $\int_0^v \sin(t^2) dt$.

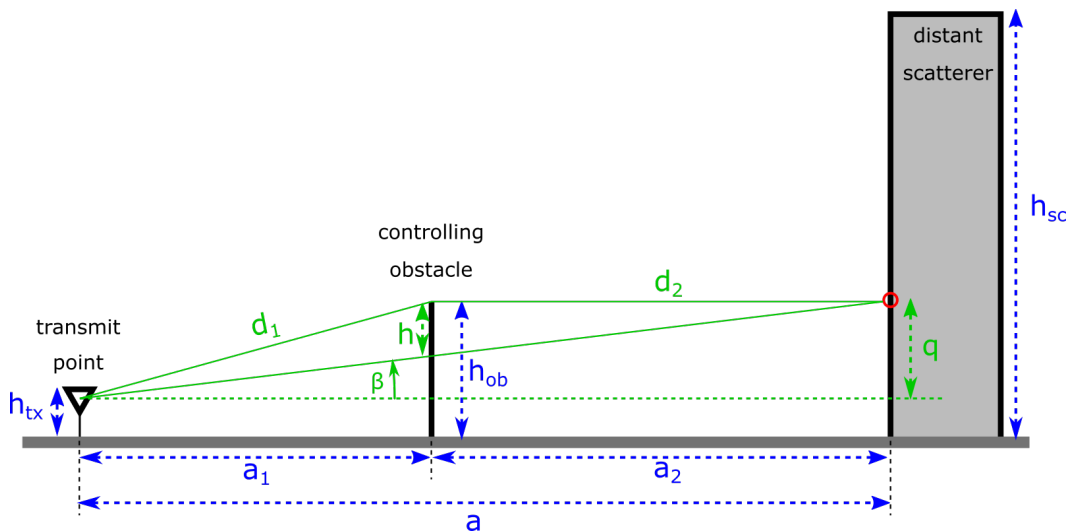
Because evaluation of the Fresnel integrals can be computationally expensive, a simple algebraic approximation for this expression has been developed (Bertoni 2000; Parsons 2000):

$$J(v) = 6.9 + 20 \log_{10} \left(\sqrt{(v - 0.1)^2 + 1} + v - 0.1 \right),$$

where the approximate expression is valid for $\nu > -0.78$. In subsequent models and code developed in this section, we use this approximation for $\nu \geq -0.78$ and use a diffraction loss value of zero $\nu < -0.78$.

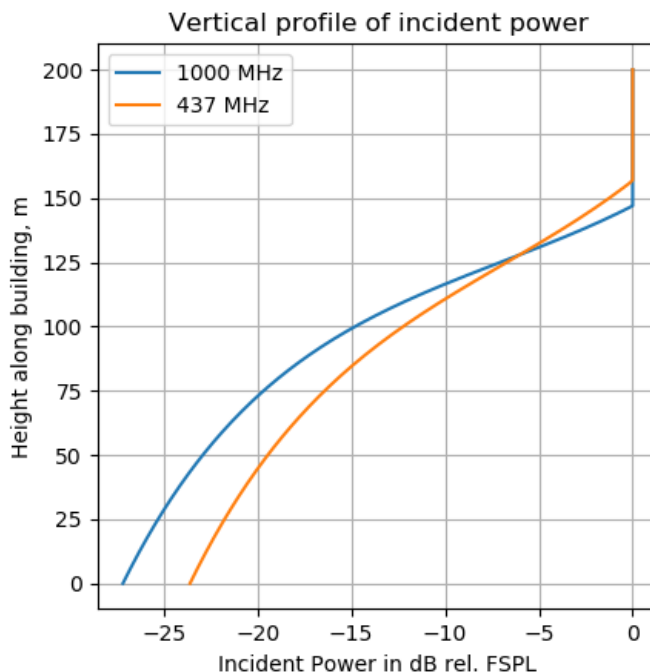
We are now ready to analyze an example vertical incident power profile based on the geometry shown in Figure 23. Our example will use an $a = 1000$ m long linear path with the transmitter at one end and a hypothetical $h_{sc} = 200$ m tall building at the other end. We place an $h_{ob} = 25$ m high controlling obstacle at $a_1 = 200$ m from the transmitter. For the purposes of this analysis, we place virtual “test” receivers at positions from ground level up to the top of our hypothetical building. One (of many) receiver positions on the building face is indicated by the red circle in Figure 23.

Figure 23. Geometry for the vertical incident power profile analysis. Structures are shown in *black* and *gray*, structure dimensions are in *blue*, key parameters for diffraction analysis are in *green*, and the *red circle* indicates the test receiver position. For simplicity, this scenario does not include a secondary obstacle.



As the test receiver takes different positions up the building face, the diffraction parameter and therefore the diffraction loss for the transmitter-to-receiver path will vary as a function of height, yielding a changing profile of incident power. Figure 24 is a plot of incident power relative to free-space path losses as a function of height.

Figure 24. The vertical profile for two different frequencies, expressed in decibels relative to free-space path loss (FSPL) of the power incident upon a hypothetical 200 m tall building. The controlling obstacle is 25 m tall, lies 200 m away from the transmitter, and is 800 m from the building.



The results in Figure 24 show that the upper 53 m of the building is fully illuminated (i.e., no diffraction losses) by the transmitter for the 1 GHz frequency and that only the upper 43 m is fully illuminated for a 437 MHz transmitter. This difference is attributable to the much larger Fresnel radius for the lower frequency, though we note that the incident power advantage for the 1 GHz signal is lost below a 128 m elevation. At all locations below this crossover point, incident power for the 437 MHz signal is stronger than that of the 1 GHz signal.

Our example geometry featured a large ($a_1 = 200$ m) separation distance between the transmitter and the controlling obstacle, so chosen to demonstrate the transition between full and partial illumination. However, this large separation is not the generally expected scenario for a ground-to-ground link. Our controlling obstacle will instead typically be within a street-width ($a_1 \sim 20$ m) of the transmitter, implying that lower-frequency signals will better illuminate distant scatterers over their entire height. As shown on the left side of Figure 24, diffraction losses are smaller at lower frequencies for our ground-based urban geometry of interest.

Based on this type of modeling for incident power, we next expand the model to predict the total power incident on the buildings in a typical urban elevation profile.

4.3.2 Total incident power for urban elevation profiles

Estimating the total incident power for the geometry of Figure 23 is a straightforward process because the location and height of the controlling obstacle and distant scatterer are known. Applying this technique to more complex geometries requires algorithms to detect and correctly apply the diffraction analysis to realistic urban elevation profiles. This section briefly describes those algorithms and discusses their results.

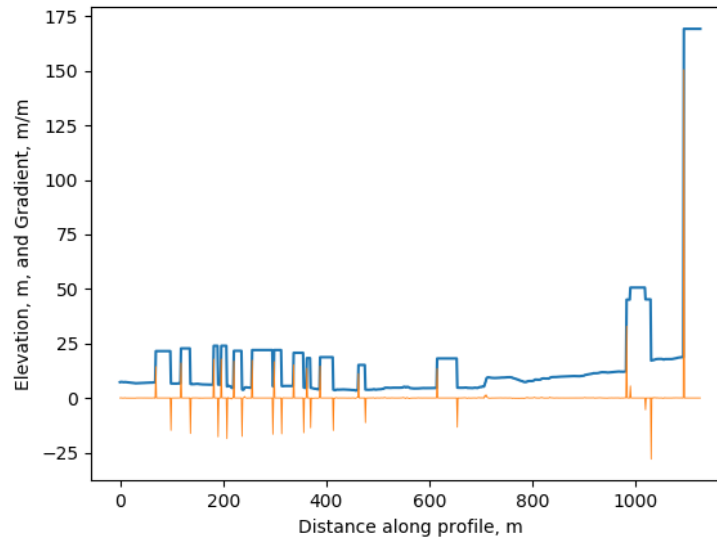
To apply the technique detailed above, we first need to identify the building faces of interest, any intervening obstacles, and their heights. Given an elevation profile $E(x)$, we can calculate the gradient $s(x)$ by differentiating with respect to distance. We assume here that $E(x)$ has been extracted from an elevation raster dataset, and thus the spatial resolution of the profile is comparable to that of the raster. Modern elevation rasters for urban areas, often derived from lidar surveys, have spatial resolutions on the order of a meter. In the case of urban terrain, the ground-to-building rooftop transitions occur over very short distances relative to the spatial resolution of $E(x)$, and thus we expect $s(x)$ to consist of a series of positive and negative spikes at building faces, separated by sections of nearly constant values associated with the ground and rooftops. The spike amplitudes are related to the rooftop height of the building above ground level. The presence and location of building faces can be readily detected using these spikes, as shown in Figure 25. Naturally occurring terrain variation values of s are generally less than 2 m/m while s for building faces routinely exceeds ± 10 m/m, and we use this latter value as a threshold for building edge detection.

The building faces of interest for diffracted illumination calculations are those closest to the transmitter point. Assuming the transmitter point lies at the zero distance point on the left-hand side of Figure 25, we see that the building faces of interest are all associated with spikes where $s(x) > 0$.

Given that the above gradient method can locate building faces of interest, we can now rank the relative slopes (from transmitter point to rooftop) of the detected faces and, for a building face of interest, determine

- the location and height of the controlling obstacle (highest transmitter-to-rooftop slope) and
- the location and height of a secondary obstacle (second highest transmitter-to-rooftop slope), which, if significantly higher than the surrounding buildings, can shadow the building face of interest.

Figure 25. Elevation (*blue*) and gradient (*orange*) profile from the North End to Downtown Boston, Massachusetts.



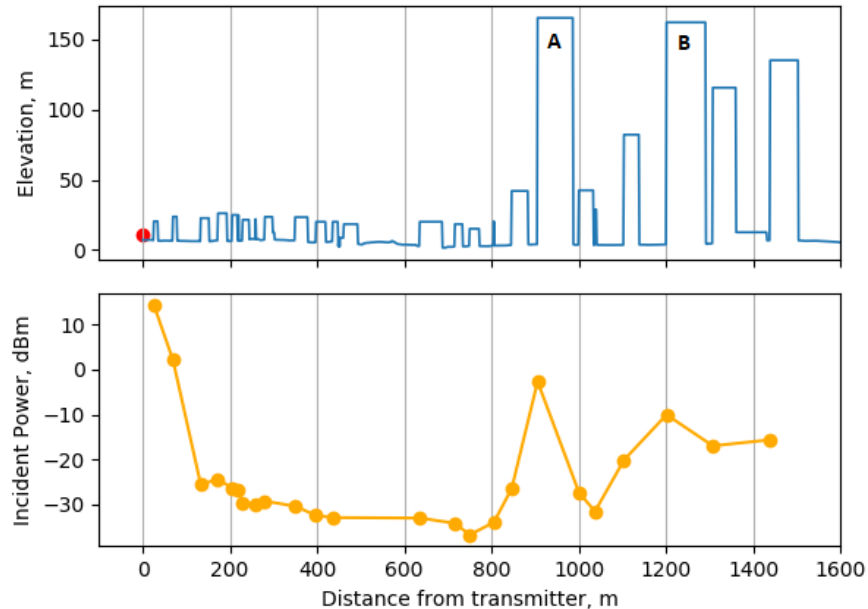
Combining the slope-rank method with the incident power calculations of section 4.3.1 allows us to analyze for incident power at each illuminated building face of interest across an urban elevation profile.

An example of such a calculation is given below in Figure 26, where the transmitter is located at the left-hand side of the plot at a height of 4 m above the ground and emits a 437 MHz signal at a power of 10 W. The elevation profile begins in the North End neighborhood (many low buildings of uniform height) and proceeds on an azimuth of 192° for just under 1.5 km, ending in the center of Downtown Boston.

The plot shows a large amount of building incident power close to the transmitter (within 100 m), which is expected: nearby buildings are strongly illuminated at street level, while more distant buildings are shadowed by those close to the transmitter. Further into the profile, we observe two roughly 150 m tall buildings, labeled A and B in Figure 26, with significant incident power. In the case of building A, it is not directly illuminated by the transmitter because the controlling obstacle is 20.5 m tall and only 25.5 m away from the transmitter: the building would need to be over

1200 m high to have any portions directly illuminated under these conditions. All of the power incident on building A is therefore diffracted from the controlling obstacle.

Figure 26. Elevation profile (*top*) and building face total incident power (*bottom*) for a path from the North End to the center of Downtown Boston. The transmitter is indicated by the *red dot*, and locations of building faces of interest are indicated by *orange dots*.



The power incident upon building B is slightly lower than the first, caused by both additional geometric spreading and signal shadowing by building A. Note that the controlling obstacle (still at 25.5 m from the transmitter) remains the same as in the previous case, and thus building A serves as the secondary obstacle for building B. Overall, then, the buildings with the highest total incident power are those with significant height and especially those at the transition between low- and high-rise neighborhoods (i.e., building A).

At this stage, we have developed methods for estimating the total RF power incident on buildings within an arbitrary urban elevation profile. This is a significant step forward because, as shown in Figure 26, we have now *identified and estimated power incident upon completely occluded scatterers*. These scatterers are not visible to either transmitter or receiver yet play a potentially critical role in defining the ground-to-ground channel and are consistent with the numerous distant-scatterer-dominated channels observed in our measurement campaign.

Expanding the above approach to analyze multiple lines of azimuth around the transmitter, we can generate 2-D maps of incident and scattered power and estimate a PDP that explicitly includes occluded scatterers. The next sections describe our efforts to achieve those goals.

4.3.3 Mapping building-incident and building-scattered power in urban terrain

The traditional method of producing 2-D maps of signal path loss is to choose a set of uniformly spaced azimuth angles around a central point of interest (a transmitter or receiver point), extract elevation profiles along each line of azimuth, and then analyze diffraction losses as a function of position along that line (Eppink and Kuebler 1994). In this section, we describe modifications to this approach to assess both free-space and diffraction losses to produce maps of building-incident and building-scattered power in urban terrain.

For free-space conditions and a bistatic geometry, the power-flux density (expressed in units of mW/m²) observed at a receiver after scattering from an object is defined as

$$p_s(d_t, d_r) = \left[\frac{P_t G_t}{4\pi d_t^2} \right] \left(\frac{\sigma^0 A}{4\pi d_r^2} \right),$$

where

- d_t = the distance from the transmitter to the scatterer (m),
- d_r = the distance from the scatterer to the receiver (m),
- P_t = the transmitter power (mW),
- G_t = the antenna gain in the direction of d_t ,
- σ^0 = the normalized radar scattering coefficient, and
- A = the total effective area of the scatterer (m²).

The term in square brackets represents the building-incident power-flux density. Additional loss factors can be included in this term as necessary to account for diffraction, absorption, and so on. In what follows, we assume that only diffraction losses are important and that we need only account for diffraction losses associated with obstacles having the largest and second-largest transmitter-to-obstacle slopes: these are called the controlling obstacle and the secondary obstacle, respectively. With these diffraction

losses included, the received power-flux density in the presence of obstacles is expressed as

$$p_{s,ob}(d_t, d_r, v_{ob}, v_{sec}) = \left[\frac{P_t G_t}{4\pi d_t^2} 10^{(J(v_{ob})+J(v_{sec}))/10} \right] \left(\frac{\sigma^0 A}{4\pi d_r^2} \right),$$

where $J(v_{ob})$ and $J(v_{sec})$ are KED losses, expressed in decibels, associated with controlling and secondary obstacles, respectively. Through the inclusion of these losses, the building-incident power-flux density, still within the square brackets, now becomes a function of height on the building face of interest.

Because the incident power varies as a function of height, determining the total building-scattered contribution to received power-flux density involves integrating the incident power-flux density over the area of the building face. In practice, this integral is evaluated as a discrete sum over the elements of building area ΔA . Thus, the total effective scatterer area on a given building face f within a line of azimuth is

$$A_f = \sum_{\text{building}} \Delta A = (\Delta\phi d_t) \sum_{\text{building}} \Delta q,$$

where

- ΔA = an element of building area (m²), summation running from ground level to building rooftop height,
- Δq = an element of building height (m) summation running from ground level to building rooftop height,
- $\Delta\phi$ = an element of azimuthal angle (radians), and
- d_t = the distance from the transmitter to the building face of interest (m).

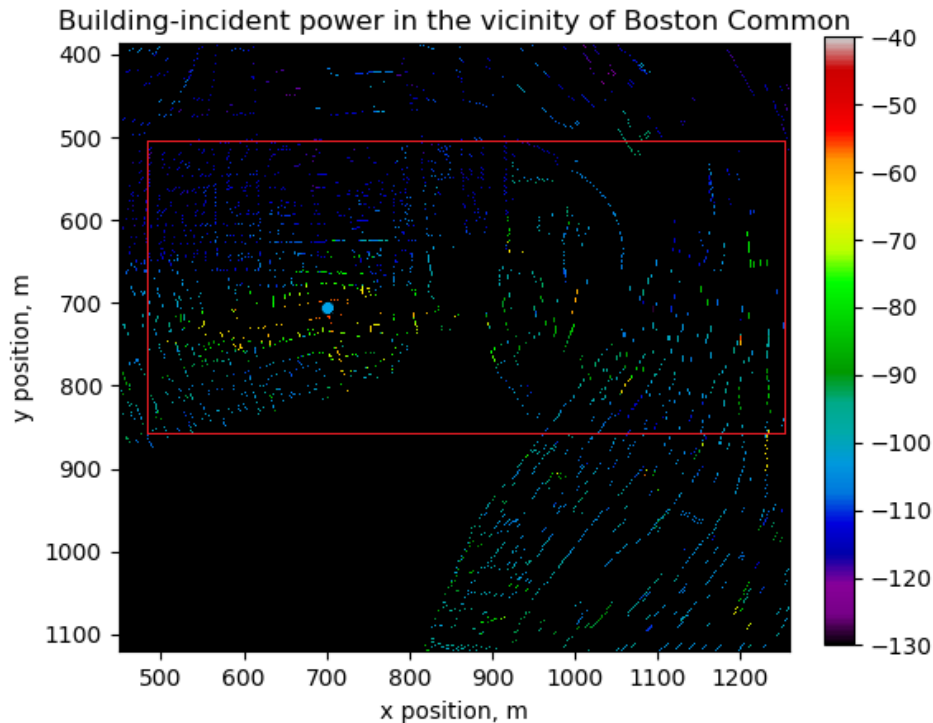
The total scattered power reaching the receiver from a given building face f along a given line of azimuth is then $P_{r,f} = p_s(d_t, d_r, v_{ob}, v_{sec})A_f$.

Nearly all of the parameters mentioned so far are known either from radio system characteristics or from the geometry of the scenario. However, the normalized radar scattering coefficient, σ^0 , has not yet been specified, and this is because relatively little is known about the diffuse scattering character of urban structures (Seidel et al. 1991; Degli-Esposti 2001). Given the wide uncertainty regarding these values and their potential dependence on

surface roughness, material properties, and other factors, we have chosen to use a simple approximation proposed by (van Rees 1987), where $\sigma^0 \cong 4$.

Taken together, the above expressions allow for the calculation and mapping of building-incident and building-scattered power-flux density. An example map of building incident power, shown in Figure 27, demonstrates high power for buildings nearby (and thus directly illuminated by) the transmitter and for distant, tall (yet occluded) buildings.

Figure 27. Map of building-incident power. The *blue circle* indicates the location of a transmitter operating at $P_t = 10$ W. *Colored pixels* indicate the total building-incident power in decibels relative to one milliwatt at a given location. The red box indicates the area shown in Fig. 28; the large blank area in the lower left is the open space of Boston Common.



In this example, the directly illuminated buildings are relatively low and surrounded by similar-height buildings, thus we do not expect these buildings to contribute significantly to the channel. The map also shows that taller, more distant buildings can have significant incident power; and we anticipate that these buildings will impact the channel.

The area within the red box in Figure 27 is shown in more detail, and with buildings, in Figure 28. This figure demonstrates the ability of our model to locate the relevant building edges and to estimate the total incident power

as a function of location and building height within a complex urban scene. Because our model is able to properly geolocate the results in a GeoTIFF format, we are able to directly use this data within standard geographical information system software, plotting RF model output over a high-resolution raster of urban elevation, including buildings.

Figure 28. Map of buildings and building-incident power. *Lighter shades of gray* indicate taller buildings, while *warmer-colored pixels* indicate higher power.

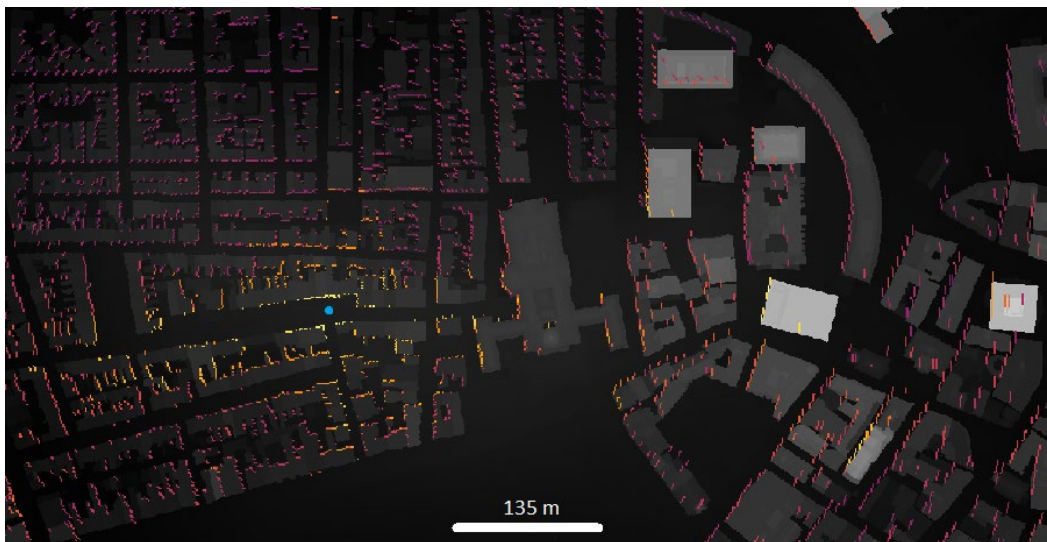


Figure 27 shows only part of the area covered by this example calculation. The whole example covered over 3 km² on a 1 m resolution digital elevation model, required 30 seconds on one core of an Intel i7-6700K operating at a 4 GHz clock speed, and captures the potential impacts of scatterers out to a 10 μ s bistatic delay time. This rapid calculation time is possible because our model ignores diffraction and shadowing losses on the scatterer-to-receiver leg, eliminating many costly evaluations of geometry and diffraction loss. In essence, our model makes the hugely simplifying assumption that the channel is most strongly influenced by the *presence* of distant scatterers and not by the details of the particular multipaths that bring scattered power down to the receiver.

The fundamental outputs of the model described above are geolocated sources of scattered RF power. This information is output in the form of a two-band raster dataset covering the region of interest: the first band describes the total scattered power contribution to the received power from a given pixel, and the second band describes the bistatic delay time associated with the pixel's position relative to the transmitter and the receiver.

The next section describes the conversion of that data into an estimate of the radio channel itself.

4.3.4 Estimating the Urban Channel for the CRREL Channel Sounder

Two facts govern the process of radio channel estimation. First, the contours of constant bistatic delay time between two points in space are in the form of 3-D ellipsoids, with the two points in question located at the foci. The intersection of this ellipsoid with the ground is well approximated by an ellipse when the ground is flat but less so in the case of significant relief, such as mountains and buildings. Second, real radio receivers have a finite bandwidth B , implying that the sampled signal at a given point in time is an average over a time roughly $1/B$ in duration.

Together, these facts imply that the power arriving within a given receiver sampling interval (associated with a given delay-time interval) is influenced by all scatterers lying within a spatial band at least c/B wide, where c is the speed of light in air. For our $B = 25$ MHz channel sounding system with no timing uncertainty, this leads to a spatial band 12 m wide. Under the more realistic assumption of at least one sampling interval worth of timing uncertainty, this expands to a band 24 m wide. Elliptical bands of this size are shown in Figure 7, which demonstrates that many buildings (some large, many small) are captured within such a band. The total measured power arriving within the sampling window has contributions from all scatterers within the band, and their importance to the channel is controlled strongly by both σ^0 and the incident power.

Under the assumption that the various scatterer contributions can be combined incoherently (i.e., no definite or persistent phase relationships exist between the different scatterers' signals), we can estimate the channel response for a given delay time, τ , by summing all of the scattered power falling within a given delay-time bin width, $\Delta\tau$, centered about τ . The measured power arriving at the receiver at delay time τ is therefore

$$P(\tau) = \sum_{\text{raster}} U_{i,j}(\tau, \Delta\tau), P_{i,j},$$

where

- i, j = the indices of a given pixel position within the raster;
- $P_{i,j}$ = the total scattered power at position i, j within the raster; and

$U(\tau, \Delta\tau)$ = a function that returns 1 if the delay time for pixel i, j has a value falling within $\tau \pm \Delta\tau$, and 0 otherwise.

This assumption of incoherence is reasonable under our hypothesis that diffuse scattering is the main contributor to the ground-to-ground channel. Summing power from the individual paths coherently might be appropriate if a few well-characterized and specular reflectors dominated the overall received signal; in practice we rarely know the geometry or material characteristics with sufficient accuracy to make the analysis worthwhile.

We simulate a finite-bandwidth receiver to accomplish this summation in our model by using the two-band raster (scattered power and bistatic delay time) produced by earlier portions of the model. The overall effect of this operation is to transform maps like Figure 27 and Figure 28 into PDPs, which characterize the impact of the propagation environment on the transmitted signal.

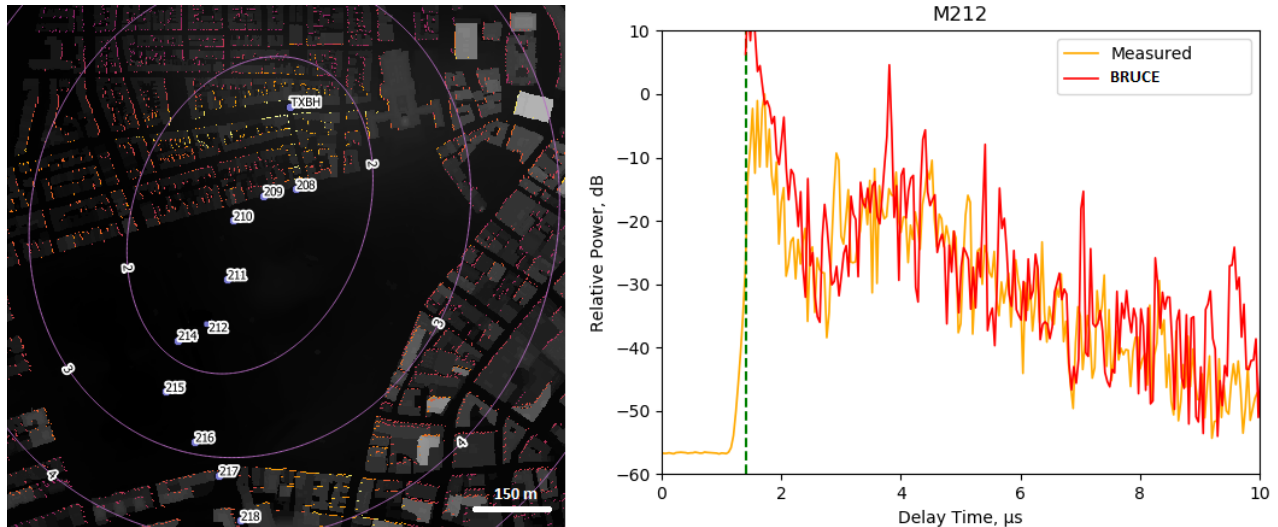
4.3.5 Comparison of measured and modeled power delay profiles

The model detailed above is called the Building Raster Urban Channel Estimator (BRUCE) because it uses a raster-based geospatial approach to the problem of urban scatterer discovery and channel estimation. In this section, we compare several measured urban channels with BRUCE results from the same locations and identify both successes and shortcomings of the model. For all results in this section, BRUCE was run with $\Delta\phi = 0.5^\circ$ and a maximum analysis range of 2 km from the transmitter. For these settings, each model run required around 3 minutes on a single CPU.

4.3.5.1 Beacon Hill to Boston Common

In our first comparison, the transmitter was located atop Beacon Hill (TXBH), and the receiver was at point M212, near the center of Boston Common. Figure 29 (*left*) maps building-incident power with overlaid 1 μs bistatic delay contours. From inspection of this map, we expect a near-LOS path to exist between the hilltop transmitter and the receiver and that the main reflections from buildings at the edge of Boston Common should fall between 3 and 4 μs . Both the near-LOS arrival (close to the free-space signal delay time denoted by a vertical dashed green line) and the Common's edge reflections are shown clearly in the PDPs on the right of Figure 29.

Figure 29. Map of building-incident power with 1 μs bistatic delay contours overlaid (*left*) and comparison of measured and modeled PDPs (*right*) for point M212. The *vertical green line* indicates the expected free-space signal delay time.

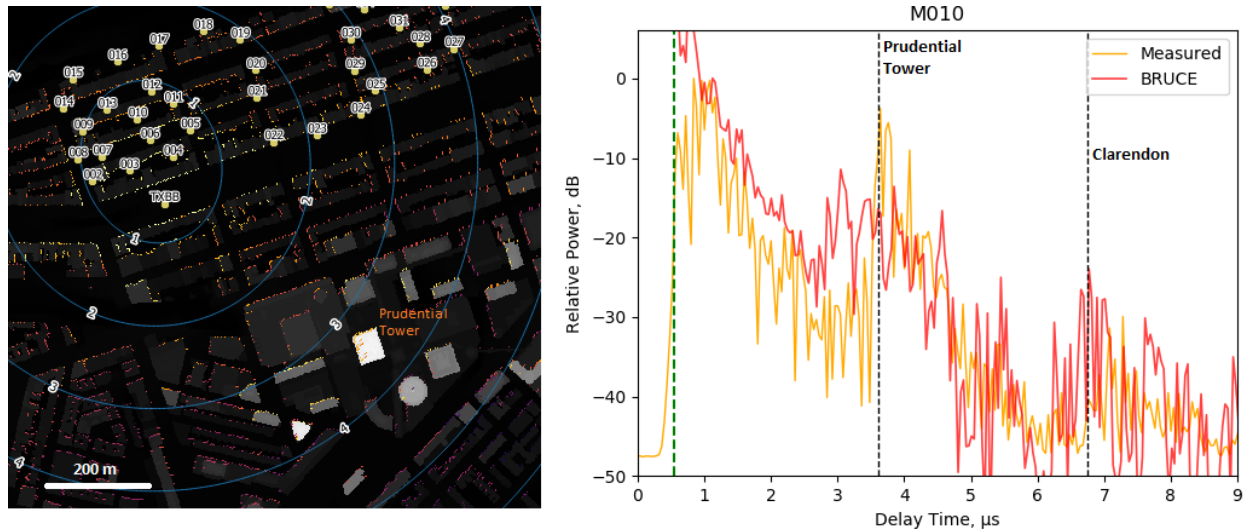


The measured and modeled PDPs have good agreement, except near the free-space signal delay time. Building-incident power is very high in the immediate vicinity of the transmitter, and thus BRUCE overestimates the received power. This shortcoming of the model is because the buildings nearby the transmitter are well illuminated but lie within a neighborhood of similar height buildings, and thus this scattered power suffers significant (but unaccounted for within BRUCE) losses en route to the receiver. This overweighting of near-transmitter scatterers can be tackled, at very considerable computational expense, by evaluating the diffraction losses between each scattering point and the receiver. For the purposes of demonstrating this modeling approach for urban channels, however, we simply note that BRUCE results within roughly 1 μs of the free-space signal delay time should be viewed with suspicion or ignored altogether.

4.3.5.2 Short-range link in Back Bay

For our second comparison, we examine a short-range, urban ground-to-ground link. The transmitter, located on Commonwealth Ave (TXBB), is separated from the receiver (M010), by a distance of 162 m and three rows of 15 m tall buildings, ensuring no LOS exists along this path. In Figure 30, we show a map of building incident power and bistatic delay-time contours for the area, along with a comparison of measured and modeled PDPs for this geometry.

Figure 30. Map of building-incident power and 1 μs delay contours (*left*) and comparison of measured and modeled PDPs (*right*) for point M010. The *black vertical dashed lines* indicate expected arrival delays for signals scattered from the Prudential Tower and 200 Clarendon.



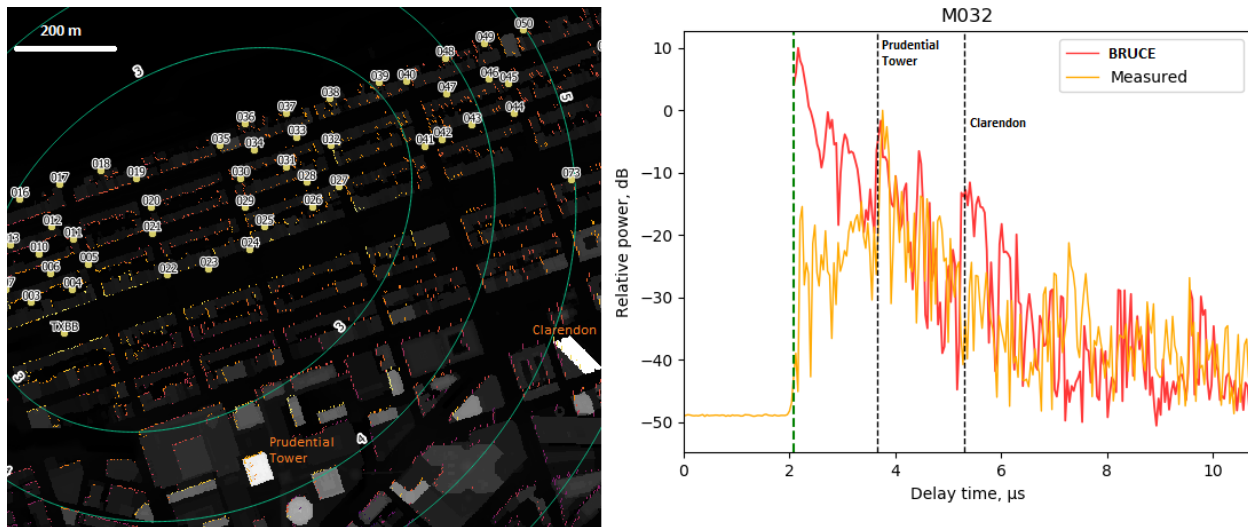
The short-delay issues with BRUCE are evident in this case as well, but overall there is good agreement between the modeled and measured channel. The PDP plot features two vertical dashed lines associated with signals scattered from the two tallest buildings in Boston: the Prudential Tower, shown on the map at 3.6 μs delay time, and 200 Clarendon, which lies off the map out at a delay time of 6.7 μs .

BRUCE does account for the tall scatterers lying from 3 out to 4.5 μs but does not capture the large signal return from the Prudential Building observed in the measured PDP at 3.6 μs . In contrast, BRUCE does predict a substantial return from 200 Clarendon, and yet the measured channel is unremarkable at 6.7 μs . We believe this discrepancy is not an accident, and we discuss this issue in section 4.3.6.

4.3.5.3 Longer-range link in Back Bay

In our final example, we examine a 630 m long NLOS link, again in Back Bay. Figure 31 shows the incident power map (*left*) and PDP comparison for this case (*right*).

Figure 31. Map of building-incident power and 1 μs delay contours (*left*) and a comparison of measured and modeled PDPs (*right*) for point M032.



As in the previous cases, BRUCE overestimates the contribution of near-transmitter buildings but generally captures the correct trend. Expected arrival times for the Prudential Tower and 200 Clarendon are shown on the PDP, where we observe significant returns from the Prudential Tower (3.7 μs) in both the measured and modeled channels and essentially no measured return at the expected delay (5.2 μs) for 200 Clarendon. Section 4.3.6 further discusses this discrepancy.

The three channel comparisons presented in this section have shown that BRUCE is able to produce reasonable estimates for various urban RF channels by accounting for power incident upon *occluded* scatterers, the most common case for a ground-to-ground radio link. Other ray-tracing-based channel models used in this work produced unrealistic channel estimates because they ignored these interactions.

Because this model operates on widely available and reasonably sized raster representations of the urban environment, it is able to complete channel estimation calculations covering over 12 km^2 in three minutes. This rapid (compared to multihour ray tracing estimates) calculation is possible because BRUCE ignores all scatterer-to-receiver losses other than geometric spreading loss. Therefore, BRUCE overestimates the impact of near-transmitter scatterers and scatterers lying in between the transmitter and receiver. For other scatterers, however, this approach appears to be a reasonable and hugely simplifying approximation.

4.3.6 The constant cross-section assumption

We return now to the most significant assumption within all of the models discussed in this work: the notion that all buildings are equally effective diffuse scatterers of RF energy and thus all have the same value of σ^0 . As discussed above, ray-tracing approaches led to poor estimates of the channel; and it is difficult to compare these estimates with measurement to investigate the possible variation of σ^0 within the urban environment.

BRUCE results appear to be good enough to directly compare with measurements and thereby shed some light on the viability of the constant σ^0 assumption and provide a means of testing our second hypothesis.

Our measured and modeled channels at MO10 and MO32 in Back Bay are within a kilometer of the two tallest buildings in New England, providing a natural laboratory with two large and approximately similar-sized scatterers with very different surface roughnesses and cladding designs, as shown in Figure 32. The Prudential Tower, built from 1960 to 1964, uses extruded square aluminum tubing to frame a regular pattern of exterior wall panels and window glass, yielding a surface relief of approximately 15 cm. The more modern 200 Clarendon, built from 1968 to 1976, features over 10,000 metal-tinted windows, each covering over 4 m² and framed by anodized aluminum. The estimated surface relief of 200 Clarendon is on the order of 3 cm. Considering the hypothesized importance of diffuse scattering on the ground-to-ground channel, we expect that these two buildings would have very different impacts on the RF channel due to differences in their ability to convert incident radiation into a diffusely scattered signal at ground level. In other words, we expect these two buildings to have different values of effective σ^0 for diffuse scattering: a relatively high value for the rough-surfaced Prudential Tower and a relatively low value for the smooth, highly conductive surfaces of 200 Clarendon.

Figure 32. Surfaces of the Prudential Tower and 200 Clarendon.



Figure 30 from measurement MO10 shows a significant return in the measured channel corresponding to scattering from the Prudential Tower at 3.6 μs . The BRUCE channel shows multiple returns associated with buildings in the vicinity of the Tower but does not predict the clear, well isolated peak observed in the measurement. There are two possible explanations, neither of which necessarily excludes the other: (1) the effective σ^0 for the Prudential Tower is higher than that of the surrounding buildings and (2) in this geometry, the Tower is illuminated from the northwest corner, normal to the delay-time contour, thus causing BRUCE to spread the building-scattered power over a wide range of delay-time bins, rather than concentrating into a narrow, obvious return.

Later in the same MO10 PDP, BRUCE predicts a clear, but spread out, return centered at 6.7 μs associated with 200 Clarendon. The temporal spread of the model result is caused by the same misorientation between the major building face and the delay-time contour direction discussed above. The measured channel at 6.7 μs shows received power within a few decibels of the instrument noise floor, indicating that this building contributes essentially nothing to the ground-to-ground channel. Given the extreme height and area presented by 200 Clarendon for this geometry, the results suggest a small σ^0 for diffuse scattering, much smaller than the constant value assumed in BRUCE.

Turning now to the results from MO32 shown in Figure 31, we observe a significant return in both the measured and modeled PDP at 3.7 μs , corresponding to the Prudential Tower. At the 5.2 μs delay time for 200 Clarendon, BRUCE predicts a significant return, but the measured channel continues its decay towards the noise floor. The simplest explanation for this behavior is that different buildings have different values of σ^0 , contrary to the assumptions of almost all models of urban radio propagation, including BRUCE.

The MO32 example presents the clearest case of two comparably sized buildings with very different diffuse radio scattering cross sections: one building (Prudential) absolutely dominates the ground-to-ground channel while another (200 Clarendon) is essentially invisible. The specular reflection from 200 Clarendon is probably substantial given its smooth and conductive surface, but only a well-positioned aircraft could observe it. The

diffuse scatter from the rough-surfaced Prudential building was an important, and often dominant, component of ground-to-ground channels measured throughout the Back Bay neighborhood.

In future work on σ^0 , we recommend using directional antennae and a controlled geometry to illuminate a known area of the building of interest. The channel would then primarily depend only on signal scattered from the building of interest, thus greatly simplifying the geometry and avoiding ambiguities created when multiple scatterers exist along the same delay-time contour. The logistics of such an experiment are not trivial, requiring rooftop access to buildings relatively nearby the building of interest. Further, due consideration must be given to the level of RF exposure to the occupants of the building under test. The results of such an experiment, however, would be straightforward to interpret if the zone of illumination was well defined.

5 Conclusions

The urban channel is complex due to the prevalence of NLOS radio links, links that depend on reflections (for canyon propagation) and diffuse scattering (for distant-scatterer contributions) for their existence. The goal of this project was to test two important and related hypotheses regarding urban radio propagation.

- Hypothesis 1: Diffuse scattering from built structures has significant impact on the ground-to-ground channel at frequencies relevant to military and first-responder operations. Our research, conducted at the upper end of the VHF/UHF bands commonly used for such communications, shows that diffuse scattering does have a significant impact on the ground-to-ground channel. Comparing our many ray-trace modeling attempts (which ignored diffuse scattering) with measured channels demonstrated that diffuse scattering is absolutely crucial to properly understanding and modeling this channel. We developed the Building Raster Urban Channel Estimator (BRUCE) to properly account for all building-incident RF power, specifically including the contributions to occluded buildings. While this model overestimates the importance of structures near the transmitter, it is able to produce far more realistic channel estimates for longer-range links where the distant-scatterer mode is important.
- Hypothesis 2: Diffuse scattering strength of urban structures depends on the surface roughness and materials present in the structures themselves. Comparing BRUCE results with the measured RF channel in Back Bay allowed us to identify specific delay-time zones where scattered signals from the Prudential Tower and 200 Clarendon were expected. The Prudential Tower was reliably observed in the measured channel as a significant, and often dominant, contributor to the channel. The 200 Clarendon building was not a strong contributor to the channel, despite BRUCE predictions that it should be. We believe that the difference in surface roughness and morphology of these two buildings is responsible for the hugely different impacts these buildings have on the ground-to-ground channel; the rougher surface of the Prudential Tower is more efficient in diffusely scattering incident RF power. A ground-based RF source incident upon the smooth, conductive surface of 200 Clarendon generates a large specular reflection into the sky,

contributing essentially nothing to the ground-to-ground channel, despite the BRUCE prediction of a substantial contribution. The model and measurement comparison suggests that different buildings have different effective σ^0 values related to the surface and material characteristics of the buildings and that these differences are large enough to be readily observable in certain urban environments.

The work presented in this report discusses urban radio propagation outside of the cellular telephone paradigm commonly discussed in the literature. The urban propagation challenges faced by Army and other Department of Defense ground operations are not the same as those of the cellular industry, where higher frequencies, higher bandwidths, and a robust, wired backhaul network is available. Our work has focused on the military and first-responder cases where these advantages are not available due to warfare, natural disaster, or both. It is therefore our hope that this work has filled some of the significant knowledge gaps still remaining in the literature outside of the cellular paradigm.

References

- Allsebrook, K., and J. D. Parsons. 1977. "Mobile Radio Propagation in British Cities at Frequencies in the v.h.f. and u.h.f. Bands." *Proceedings of the Institution of Electrical Engineers* 124 (2): 95–102. <https://doi.org/10.1049/piee.1977.0016>.
- Almers, P., E. Bonek, A. Burr, N. Czink, M. Debbah, V. Degli-Esposti, H. Hofstetter, P. Kyösti, D. Laurenson, G. Matz, A. F. Molisch, C. Oestges, and H. Özcelik. 2007. "Survey of Channel and Radio Propagation Models for Wireless MIMO Systems." *EURASIP Journal on Wireless Communications and Networking* 2007:019070. <https://doi.org/10.1155/2007/19070>.
- Beckmann, Petr. 1968. *The Depolarization of Electromagnetic Waves*. Boulder, CO: Golem Press.
- Bertoni, H. L. 2000. *Radio Propagation for Modern Wireless Systems*. Upper Saddle River, NJ: Prentice-Hill PTR.
- Bertoni, H. L., W. Honcharenko, L. R. Macel, and H. Xia. 1994. "UHF Propagation Prediction for Wireless Personal Communications." *Proceedings of the IEEE* 82 (9): 1333–1359.
- Braun, W. R., and U. Dersch. 1991. "A Physical Mobile Radio Channel Model." *IEEE Transactions on Vehicular Technology* 40 (2): 472–482.
- Breton, D. J., C. E. Haedrich, and G. Hoch. 2019. "Measured Characteristics of Urban Depolarization in Ground-to-Ground UHF Wideband Channels." Presented at the 2019 National Radio Science Meeting, Boulder, Colorado, January 2019.
- Breton, D. J., C. E. Haedrich, M. J. Kamrath, and D. K. Wilson. 2019. "Street-Scale Mapping of Urban Radio Frequency Noise at Very High Frequency and Ultra High Frequency." *Radio Science* 54 (11): 934–948. <https://doi.org/10.1029/2019RS006893>.
- Breton, D. J., S. S. Streeter, and G. R. Hoch. 2018. "Comparison of Roof Top- and Ground-to-Ground Urban Propagation of Wideband UHF Signals." In *Proceedings, 2018 IEEE International Symposium on Antennas and Propagation & USNC/URSI National Radio Science Meeting*, 8–13 July, Boston, MA, 75–76. <https://doi.org/10.1109/APUSNCURSINRSM.2018.8609176>.
- Cheng, X., Y. Li, B. Ai, X. Yin, and Q. Wang. 2015. "Device-to-Device Channel Measurements and Models: A Survey." *IET Communications* 9 (3): 312–325. <https://doi.org/10.1049/iet-com.2014.0442>.
- Cox, D. 1973. "910 MHz Urban Mobile Radio Propagation: Multipath Characteristics in New York City." *IEEE Transactions on Communications* 21 (11): 1188–1194. <https://doi.org/10.1109/TCOM.1973.1091571>.
- Cuckovic, Z. 2016. "Advanced Viewshed Analysis: A Quantum GIS Plug-In for the Analysis of Visual Landscapes." *Journal of Open Source Software* 1 (4): 32. <https://doi.org/10.21105/joss.00032>.

- De Weck, J.-P., P. Merki, and R. W. Lorenz. 1988. "Power Delay Profiles Measured in Mountainous Terrain (Radiowave Propagation)." In *Proceedings, 38th IEEE Vehicular Technology Conference*, 15–17 June, Philadelphia, PA, 105–112. <https://doi.org/10.1109/VETEC.1988.195344>.
- Degli-Esposti, V. 2001. "A Diffuse Scattering Model for Urban Propagation Prediction." *IEEE Transactions on Antennas and Propagation* 49 (7): 1111–1113. <https://doi.org/10.1109/8.933491>.
- Degli-Esposti, V., and H. L. Bertoni. 1999. "Evaluation of the Role of Diffuse Scattering in Urban Microcellular Propagation." In *Gateway to 21st Century Communications Village, VTC 1999-Fall, IEEE VTS 50th Vehicular Technology Conference (Cat. No.99CH36324)*, 19–22 September, Amsterdam, The Netherlands, 3:1392–1396. <https://doi.org/10.1109/VETECF.1999.801491>.
- Degli-Esposti, V., F. Fuschini, E. M. Vitucci, and G. Falciasecca. 2007. "Measurement and Modelling of Scattering from Buildings." *IEEE Transactions on Antennas and Propagation* 55 (1): 143–153. <https://doi.org/10.1109/TAP.2006.888422>.
- Degli-Esposti, V., V. Kolmonen, E. M. Vitucci, and P. Vainikainen. 2011. "Analysis and Modeling on Co- and Cross-Polarized Urban Radio Propagation for Dual-Polarized MIMO Wireless Systems." *IEEE Transactions on Antennas and Propagation* 59 (11): 4247–4256. <https://doi.org/10.1109/TAP.2011.2164226>.
- Devasirvatham, D. M. J. 1988. "Radio Propagation Studies in a Small City for Universal Portable Communications." In *38th IEEE Vehicular Technology Conference*, 15–17 June, Philadelphia, PA, 100–104. <https://doi.org/10.1109/VETEC.1988.195343>.
- Deygout, J. 1966. "Multiple Knife-Edge Diffraction of Microwaves." *IEEE Transactions on Antennas and Propagation* 14 (4): 480–489.
- Driessen, P. F. 1992. "Multipath Delay Characteristics in Mountainous Terrain at 900 MHz." In *Proceedings, Vehicular Technology Society 42nd VTS Conference - Frontiers of Technology*, 10–13 May, Denver, CO, 520–523. <https://doi.org/10.1109/VETEC.1992.245342>.
- Durgin, G. D. 2009. "The Practical Behavior of Various Edge-Diffraction Formulas." *IEEE Antennas and Propagation Magazine* 51 (3): 24–35. <https://doi.org/10.1109/MAP.2009.5251189>.
- Durgin, G. D., V. Kukshya, and T. S. Rappaport. 2003. "Wideband Measurements of Angle and Delay Dispersion for Outdoor and Indoor Peer-to-Peer Radio Channels at 1920 MHz." *IEEE Transactions on Antennas and Propagation* 51 (5): 936–944. <https://doi.org/10.1109/TAP.2003.811494>.
- Eppink, D., and W. Kuebler. 1994. *TIREM/SEM Handbook*. ECAC-HDBK-93-076. Annapolis, MD: Department of Defense. <https://apps.dtic.mil/dtic/tr/fulltext/u2/a296913.pdf>.
- Haedrich, C. E., and D. J. Breton. 2019. *Measuring Very High Frequency and Ultrahigh Frequency Radio Noise in Urban Environments: A Mobile Measurement System for Radio-Frequency Noise*. ERDC/CRREL TR-19-8. Hanover, NH: U.S. Army Engineer Research Development Center, Cold Regions Research and Engineering Laboratory. <http://dx.doi.org/10.21079/11681/33290>.

- Hata, M. 1980. "Empirical Formula for Propagation Loss in Land Mobile Radio Services." *IEEE Transactions on Vehicular Technology* 29 (3): 317–325. <https://doi.org/10.1109/T-VT.1980.23859>.
- Ikegami, F., and S. Yoshida. 1980. "Analysis of Multipath Propagation Structure in Urban Mobile Radio Environments." *IEEE Transactions on Antennas and Propagation* 28 (4): 531–37. <https://doi.org/10.1109/TAP.1980.1142372>.
- International Telecommunications Union. 2019. *Multipath Propagation and Parameterization of Its Characteristics*. Recommendation P.1407-7. Geneva: International Telecommunications Union. <https://www.itu.int/rec/R-REC-P.1407-7-201908-I/en>.
- Izraelevitz, David. 2003. "A Fast Algorithm for Approximate Viewshed Computation." *Photogrammetric Engineering and Remote Sensing* 69 (7): 767–774. <https://doi.org/10.14358/PERS.69.7.767>.
- Kalliola, K., H. Laitinen, P. Vainikainen, M. Toeltsch, J. Laurila, and E. Bonek. 2003. "3-D Double-Directional Radio Channel Characterization for Urban Macrocellular Applications." *IEEE Transactions on Antennas and Propagation* 51 (11): 3122–3133. <https://doi.org/10.1109/TAP.2003.816393>.
- Kozono, S., and A. Taguchi. 1993. "Mobile Propagation Loss and Delay Spread Characteristics with a Low Base Station Antenna on an Urban Road." *IEEE Transactions on Vehicular Technology* 42 (1): 103–109. <https://doi.org/10.1109/25.192393>.
- Laurila, J., K. Kalliola, M. Toeltsch, K. Hugl, P. Vainikainen, and E. Bonek. 2002. "Wideband 3D Characterization of Mobile Radio Channels in Urban Environment." *IEEE Transactions on Antennas and Propagation* 50 (2): 233–243. <https://doi.org/10.1109/8.998000>.
- Long, M. W. 2001. *Radar Reflectivity of Land and Sea*. 3rd ed. Boston, MA: Artech House.
- Meijerink, A., and A. F. Molisch. 2014. "On the Physical Interpretation of the Saleh–Valenzuela Model and the Definition of Its Power Delay Profiles." *IEEE Transactions on Antennas and Propagation* 62 (9): 4780–4793. <https://doi.org/10.1109/TAP.2014.2335812>.
- Parsons, J. D. 2000. *The Mobile Radio Propagation Channel*. 2nd ed. Chichester, UK: Wiley.
- Paulson, A. 2019. "Precision Geolocation of Propagation Data Using GPS and Data Fusion." In *Proceedings of the 2019 IEEE International Symposium on Electromagnetic Compatibility, Signal & Power Integrity*, 22–26 July, New Orleans, LA, 469–474. <https://doi.org/10.1109/ISEMC.2019.8825198>.
- Rappaport, T. S. 2002. *Wireless Communications: Principles and Practice*. 2nd ed. Upper Saddle River, NJ: Prentice-Hill PTR.
- Saleh, A. A. M., and R. Valenzuela. 1987. "A Statistical Model for Indoor Multipath Propagation." *IEEE Journal on Selected Areas in Communications* 5 (2): 128–137. <https://doi.org/10.1109/JSAC.1987.1146527>.

- Salous, S. 2013. *Radio Propagation Measurement and Channel Modelling*. West Sussex, UK: Wiley.
- Seidel, S. Y., T. S. Rappaport, S. Jain, M. L. Lord, and R. Singh. 1991. "Path Loss, Scattering and Multipath Delay Statistics in Four European Cities for Digital Cellular and Microcellular Radiotelephone." *IEEE Transactions on Vehicular Technology* 40 (4): 721–730. <https://doi.org/10.1109/25.108383>.
- Streeter, S. S., D. J. Breton, and J. M. Corgan. 2018. "Measuring the Non-Line-of-Sight Ultra-High-Frequency Channel in Mountainous Terrain : A Spread-Spectrum, Portable Channel Sounder." ERDC/CRREL TR-18-3. Hanover, NH: U.S. Army Engineer Research Development Center, Cold Regions Research and Engineering Laboratory. <http://dx.doi.org/10.21079/11681/26602>.
- Turin, G. L., F. D. Clapp, T. L. Johnston, S. B. Fine, and D. Lavry. 1972a. "A Statistical Model of Urban Multipath Propagation." *IEEE Transactions on Vehicular Technology* 21 (1): 1–9. <https://doi.org/10.1109/T-VT.1972.23492>.
- . 1972b. "A Statistical Model of Urban Multipath Propagation." *IEEE Transactions on Vehicular Technology* 21 (1): 1–9.
- Van Rees, J. 1987. "Measurements of the Wide-Band Radio Channel Characteristics for Rural, Residential, and Suburban Areas." *IEEE Transactions on Vehicular Technology* 36 (1): 2–6. <https://doi.org/10.1109/T-VT.1987.24090>.
- Vassiliou, M. S., J. R. Agre, S. Shah, and T. MacDonald. 2013. "Crucial Differences between Commercial and Military Communications Technology Needs: Why the Military Still Needs Its Own Research." In *MILCOM 2013 - 2013 IEEE Military Communications Conference*, 18–20 November 2013, San Diego, CA, 342–347. <https://doi.org/10.1109/MILCOM.2013.66>.
- Vitucci, E. M., F. Mani, V. Degli-Esposti, and C. Oestges. 2012. "Polarimetric Properties of Diffuse Scattering From Building Walls: Experimental Parameterization of a Ray-Tracing Model." *IEEE Transactions on Antennas and Propagation* 60 (6): 2961–2969. <https://doi.org/10.1109/TAP.2012.2194683>.
- Young, W. F., K. A. Remley, C. L. Holloway, G. Koepke, D. Camell, J. Ladbury, and C. Dunlap. 2014. "Radiowave Propagation in Urban Environments with Application to Public-Safety Communications." *IEEE Antennas and Propagation Magazine* 56 (4): 88–107. <https://doi.org/10.1109/MAP.2014.6931660>.

REPORT DOCUMENTATION PAGE

Form Approved
OMB No. 0704-0188

Public reporting burden for this collection of information is estimated to average 1 hour per response, including the time for reviewing instructions, searching existing data sources, gathering and maintaining the data needed, and completing and reviewing this collection of information. Send comments regarding this burden estimate or any other aspect of this collection of information, including suggestions for reducing this burden to Department of Defense, Washington Headquarters Services, Directorate for Information Operations and Reports (0704-0188), 1215 Jefferson Davis Highway, Suite 1204, Arlington, VA 22202-4302. Respondents should be aware that notwithstanding any other provision of law, no person shall be subject to any penalty for failing to comply with a collection of information if it does not display a currently valid OMB control number. PLEASE DO NOT RETURN YOUR FORM TO THE ABOVE ADDRESS.

| | | | | | | |
|--|------------------------------------|-------------------------------------|--|--------------------------------------|---|--|
| 1. REPORT DATE (DD-MM-YYYY) July 2020 | | | 2. REPORT TYPE Final Report | | 3. DATES COVERED (From - To) | |
| 4. TITLE AND SUBTITLE The Urban Ground-to-Ground Radio-Frequency Channel: Measurement and Modeling in the Ultrahigh Frequency Band | | | | | 5a. CONTRACT NUMBER | |
| | | | | | 5b. GRANT NUMBER | |
| | | | | | 5c. PROGRAM ELEMENT 611102 | |
| 6. AUTHOR(S) Daniel J. Breton, Caitlin E. Haedrich, Garrett R. Hoch, Samuel S. Streeter, and Michele L. Maxson | | | | | 5d. PROJECT NUMBER T24 and 52C | |
| | | | | | 5e. TASK NUMBER | |
| | | | | | 5f. WORK UNIT NUMBER | |
| 7. PERFORMING ORGANIZATION NAME(S) AND ADDRESS(ES) U.S. Army Engineer Research and Development Center (ERDC) Cold Regions Research and Engineering Laboratory (CRREL) 72 Lyme Road Hanover, NH 03755-1290 | | | | | 8. PERFORMING ORGANIZATION REPORT NUMBER ERDC/CRREL TR-20-8 | |
| 9. SPONSORING / MONITORING AGENCY NAME(S) AND ADDRESS(ES) U.S. Army Corps of Engineers Washington, DC 20314-1000 | | | | | 10. SPONSOR/MONITOR'S ACRONYM(S) USACE | |
| | | | | | 11. SPONSOR/MONITOR'S REPORT NUMBER(S) | |
| 12. DISTRIBUTION / AVAILABILITY STATEMENT Approved for public release; distribution is unlimited. | | | | | | |
| 13. SUPPLEMENTARY NOTES ERDC 6.1 Basic Research | | | | | | |
| 14. ABSTRACT Ground-to-ground radio communication and sensing within the urban environment is challenging because line of sight between transmitter and receiver is rarely available. Therefore, radio links are often critically reliant on reflection and scattering from built structures. Little is known about the scattering strength of different buildings or whether such differences are important to the urban ground-to-ground channel. We tested the hypotheses that (1) diffuse scattering from built structures significantly impacts the urban channel and (2) scattering strength of urban structures varies with surface roughness and materials. We tested these hypotheses by measuring urban channels in Concord, New Hampshire, and Boston, Massachusetts, and via channel-modeling efforts with three-dimensional representations of the urban environment. Direct comparison between measured and modeled channels suggest that both of these hypotheses are true. Further, it appears that ray-tracing approaches underestimate the complexity of urban channels because these approaches lack the physical processes to correctly assess the power incident on and scattered from built structures. We developed a radio-geospatial model that better accounts for incident power on both directly visible and occluded buildings and show that our model predictions compare more favorably with measured channels than those channels predicted via typical ray-tracing approaches. | | | | | | |
| 15. SUBJECT TERMS Buildings, Cities and towns, Diffuse, Model, Propagation, Radio frequency, Radio Measurements, Scattering, Ultrahigh-frequency, Urban | | | | | | |
| 16. SECURITY CLASSIFICATION OF: | | | 17. LIMITATION OF ABSTRACT SAR | 18. NUMBER OF PAGES 83 | 19a. NAME OF RESPONSIBLE PERSON | |
| a. REPORT Unclassified | b. ABSTRACT Unclassified | c. THIS PAGE Unclassified | | | 19b. TELEPHONE NUMBER (include area code) | |